TOPICAL REVIEW

Gyrokinetic simulations of turbulent transport

IOP Publishing and International Atomic Energy Agency Nuclear Fusion

Nucl. Fusion **50** (2010) 043002 (30pp) doi:10.1088/0029-5515/50/4/043002

TOPICAL REVIEW

Gyrokinetic simulations of turbulent transport

X. Garbet[1], Y. Idomura[2], L. Villard[3] and T.H. Watanabe[4]

[1] CEA, IRFM, F-13108 Saint Paul Lez Durance, France
[2] Japan Atomic Energy Agency, Higashi-Ueno 6-9-3, Taitou, Tokyo 110-0015, Japan
[3] Ecole Polytechnique Fédérale de Lausanne (EPFL), Centre de Recherches en Physique des Plasmas, Association Euratom-Confédération Suisse, CH-1015 Lausanne, Switzerland
[4] National Institute for Fusion Science, Toki, Gifu 509-5292, Japan

Received 3 March 2008, accepted for publication 8 February 2010
Published 16 March 2010
Online at stacks.iop.org/NF/50/043002

Abstract
This overview is an assessment of the gyrokinetic framework and simulations to compute turbulent transport in fusion plasmas. It covers an introduction to the gyrokinetic theory, the principal numerical techniques which are being used to solve the gyrokinetic equations, fundamentals in gyrokinetic turbulence and the main results which have been brought by simulations with regard to transport in fusion devices and fluctuation measurements.

PACS numbers: 52.30.Gz, 52.35.Ra, 52.55.Fa, 52.55.Hc, 52.65.Tt, 52.65.Rr, 52.25.Fi, 52.25.Dg

(Some figures in this article are in colour only in the electronic version)

1. Introduction

Understanding and predicting turbulent transport is a key issue on the way towards commercially viable fusion reactors. Indeed turbulence controls the confinement properties of any magnetically confined plasma. The understanding of turbulent transport has made tremendous progress thanks to a wealth of analytical results, numerical simulations and dedicated experiments. A decisive step has been made with the development of the gyrokinetic framework for describing turbulence, and also with the emergence of numerical codes able to solve the set of gyrokinetic equations. These numerical tools have played an important role in clarifying a number of pending issues in turbulent transport. For previous reviews of the subject, see, e.g., [1–3]. This overview presents an assessment of the main advances in gyrokinetic theory and computing of turbulence.

This grand tour starts with a presentation of some basics in gyrokinetic theory. In principle, the description of plasma turbulence requires to solve six dimensional Vlasov (or Fokker–Planck) equations for each species, coupled to Maxwell equations [4]. In essence, the gyrokinetic theory aims at reducing the original 6D kinetic problem into a 5D problem (typically three coordinates of gyro-centres, one parallel velocity or energy coordinate and the adiabatic invariant which is a motion invariant). This 5D problem is easier to solve than the full kinetic one, thanks to the elimination of the fast cyclotron time scale. This transform, essentially a change of coordinates, is licit when the frequency of fluctuations is smaller than cyclotron frequencies, an ordering which is well justified in most fusion devices. However, this operation requires some care. This is due for one part to the Hamiltonian character of trajectories, which must be conserved in that transform, even if non-canonical coordinates are used. Moreover, Maxwell equations must be written with care. Indeed, particle charge and current densities, which are the sources of the Maxwell equations, differ from their gyro-centre counterparts. The differences are polarization and magnetization terms which have to be accounted for in a proper way. An extensive overview was published recently [5], which describes this transform to all orders in the expansion parameter (essentially the normalized gyroradius ρ_*, which is the ratio of the Larmor radius to the minor radius of the plasma). This rather technical step is summarized in this overview, and illustrated by a description of the equations at order one in ρ_*.

Once the equations to be solved are properly written, the task is not over yet. Indeed, solving 5D gyrokinetic Vlasov (or Fokker–Planck) equations for each species is a challenge. This difficulty is made even harder due to the complex geometry and boundary conditions that have to be implemented in the modelling. Moreover, the high dimensionality of the problem and its intrinsic nonlinear character imposes the use

of a large number of grid points or markers. This in turn implies that gyrokinetic codes require state-of-the-art high performance computing (HPC) techniques and must run on highly parallelized computers. Various numerical schemes have been explored until now, which can be classified as Lagrangian, Eulerian and semi-Lagrangian. Each approach has its advantages and drawbacks, which are summarized in this survey. The difficulty is not only about developing smart numerical schemes but also code parallelization, data analysis and visualization. Overall, it is certainly fair to say that gyrokinetics has triggered activity in applied mathematics and computer science that extends well beyond plasma physics. Given the complexity of the problem, verification is an issue. This is done by comparing simulations with exact analytical results, typically linear stability, dynamics of poloidal flows and other available tests. Also, conservation laws must be satisfied, principally energy conservation and entropy production balance. Finally, extensive code benchmarking has been done in the past, in order to cross-check the various numerical tools. Once this is done, a gyrokinetic code can be considered as 'verified', and ready for validation, i.e. comparison with experimental observations, and/or to explore a given theoretical problem.

Obviously, gyrokinetic theory is intimately entangled in the physics of turbulent transport in magnetized fusion plasmas. Hence a survey of the fundamentals of plasma turbulence is in order, in relation to the results brought by gyrokinetic simulations. The present overview is focused on core turbulence, since the kinetic simulation of edge plasma turbulence is just commencing. Core turbulence is triggered by microinstabilities, driven by density, temperature and sometimes velocity gradients. Tradition is to separate between electron and ion driven instabilities, and also to discriminate the various players through their characteristic wavelengths, usually compared with the ion and electron gyroradii, respectively. This is the purpose of linear gyrokinetic stability analysis, which is now well established. The nonlinear regime, i.e. turbulence, is somewhat more demanding, since this is still largely an open problem. Nevertheless, a picture of magnetized plasma turbulence has emerged. In particular, it is now well established that turbulence self-organizes via the generation of structures which feed back on the turbulence background. The most known are zonal flows, which are connected to fluctuations of the flux-surface-averaged poloidal velocity. Zonal flows are generated by turbulence and back react on turbulence via vortex shearing and convection from locally stable to unstable regions. Although this subject has been covered by an extensive overview [6], some important features specific to gyrokinetics are recalled and commented on here. Streamers, which are elongated convective cells in the radial direction, also play an important role in turbulence self-organization. In the same category, avalanches (fronts) participate in the relaxation of profiles, and contribute to profile stiffness. Finally, as in neutral fluid turbulence, dimensionless scaling laws turn out to be useful. In principle, there exists a large number of dimensionless numbers in magnetized plasmas. Nevertheless, three parameters appear to play a prominent role, namely, the normalized gyroradius, plasma β and collisionality. The dependence on these parameters has been extensively studied with the help of gyrokinetics and compared with the data coming from dedicated experiments. Although many issues remain unresolved, impressive progress has been made, and has, for instance, allowed the constraining of scaling laws for the ITER project.

One important aim of gyrokinetic theory is to predict turbulent transport in fusion plasmas. Hence validation is a central issue. This is done mainly in two ways. This first one is based on a comparison of calculated and measured turbulent fluxes (or transport coefficients). The second approach consists in confronting other statistically averaged quantities such as the turbulence intensity, spectra or bicoherence to experimental data, whenever available. Obviously the latter is more demanding than the former, but not always possible as it requires the implementation of synthetic diagnostics, and of course appropriate fluctuation diagnostics in fusion devices. Regarding the various transport channels, the understanding of ion heat transport in low β plasmas can be considered as mature. In fact, ion turbulent transport is now considered as a reference for testing codes. The understanding of electron heat transport has also made progress. The role of sub-ion gyroradius instabilities has been debated for some time, in particular regarding the effect of streamers and the relative contributions of small and large scales to turbulent transport. This issue has been settled with the recent achievements of turbulence simulations covering a large range of spatial scales and combining both ion and electron temperature gradient-driven instabilities. Particle and impurity transport is another important field of research. Theory and simulations of main ion transport have now reached some maturity and a rather clear picture, though incomplete, has emerged with time. The situation is less clear for impurity transport, in particular regarding the mass and charge number scaling, and also the direction of pinch velocities. Finally, momentum transport has started being addressed recently, and is less well assessed. The results summarized in this review should be considered as a snapshot of the present situation, and will certainly evolve in the future. The question of improved confinement and transport barriers is also of importance. It is now well established that shear flows and the optimization of the magnetic configuration, in particular via magnetic shear, can reduce turbulent transport. Other mechanisms are possible, but less generic. The stabilizing effect of shear flow is now well documented. Still the mechanisms that determine the mean shear flow dynamics, i.e. the radial electric field, are not fully mastered. Regarding the effect of the magnetic configuration, the situation is even less satisfactory. In particular, the puzzling role of low order rational resonant surfaces at the onset of transport barriers remains to be clarified. Several explanations have been proposed for this behaviour, but remain to be compared with experiment. This overview ends with a brief summary of comparison with fluctuation measurements in fusion devices. This subject started only recently. First results are quite encouraging and will certainly trigger further work.

The reader will certainly notice that the majority of works cited in this review deal with tokamaks. This reflects the current situation where most of the fusion research worldwide is devoted to that particular type of confinement. Another reason is that the first generations of 3D systems were dominated by single particle confinement and neoclassical transport considerations. With the advent of advanced

concepts such as drift-optimized, pseudo- or quasi-symmetric configurations, the neoclassical transport can be reduced to a level comparable to that of tokamaks and therefore turbulence-driven transport is also becoming a concern for such systems. The physical model, the numerical methods and several of the basic physics phenomena discussed in the paper are quite generically applicable to any magnetic confinement configuration. Certain specificities, related in particular to the increased complexity posed by the breaking of symmetry in 3D systems, are nevertheless pointed out at several places in the paper.

The paper is organized as follows. Section 2 presents the physical model for gyrokinetic turbulence. Numerical issues are addressed in section 3, while fundamentals of gyrokinetics are commented on in section 4. Finally, the input brought by gyrokinetic simulations into the understanding of turbulent transport is addressed in section 5. A conclusion follows.

2. Physical model

2.1. Kinetic model

In principle, a plasma dynamics may be completely described by the Newton–Maxwell system or the Klimontovich–Maxwell system. However, a fusion plasma typically consists of $\sim 10^{20}\,\mathrm{m}^{-3}$ ions and electrons, and it is unrealistic to trace all of them even with the most powerful computers in the present day and any foreseeable future. Therefore, instead of solving all the particle motion for each species, a statistical approach is introduced to describe a plasma by a particle distribution function. In a high temperature fusion plasma with $\sim$10 keV, the kinetic energy is much larger than the average potential energy between particles, which means that particles are weakly coupled. In a weakly coupled plasma, multiple particle correlations involving three particles or more are neglected, and two particle interaction is reduced to a collision operator $C(f_{s'}, f_s)$ for a single particle distribution function $f_s(\boldsymbol{q}, \boldsymbol{p})$ in six dimensional (6D) phase space $\boldsymbol{Z}_{\mathrm{CC}} = (\boldsymbol{q}, \boldsymbol{p})$ [4], where $\boldsymbol{q}$ and $\boldsymbol{p}$ are the position and momentum of a particle, respectively. As a result, an evolution equation of f_s is given by the Boltzmann equation,

$$\frac{\mathrm{D}f_s}{\mathrm{D}t} \equiv \frac{\partial f_s}{\partial t} + \{f_s, H_s\} = C(f_{s'}, f_s), \tag{1}$$

where $\{\cdot, \cdot\}$ is the Poisson bracket in the canonical coordinates $(\boldsymbol{q}, \boldsymbol{p})$,

$$\{F, G\} = \frac{\partial F}{\partial q_i}\frac{\partial G}{\partial p_i} - \frac{\partial F}{\partial p_i}\frac{\partial G}{\partial q_i}, \tag{2}$$

and $H_s(\boldsymbol{q}, \boldsymbol{p})$ is the Hamiltonian of collisionless single particle motion,

$$H_s(\boldsymbol{q}, \boldsymbol{p}) = \frac{1}{2m_s}\left|\boldsymbol{p} - \frac{e_s}{c}\boldsymbol{A}\right|^2 + e_s\phi. \tag{3}$$

Here, e_s and m_s are the charge and mass of the particle species s, c is the velocity of light, ϕ is the electrostatic potential and $\boldsymbol{A}$ is the vector potential for the magnetic field $\boldsymbol{B} = \nabla \times \boldsymbol{A}$. In considering microturbulence, a collisionless model is often used, because the collision frequency is much lower than characteristic frequencies of turbulent fluctuations such as drift waves and kinetic Alfvén waves (see figure 1). In the collisionless limit with $C(f_{s'}, f_s) = 0$, equation (1) yields the Vlasov equation or the collisionless Boltzmann equation,

$$\frac{\mathrm{D}f_s}{\mathrm{D}t} \equiv \frac{\partial f_s}{\partial t} + \{f_s, H_s\} = 0. \tag{4}$$

By taking the velocity moments of f_s, the particle density n_s and the current density $\boldsymbol{j}_s$ in the configuration space $\boldsymbol{q}$ are obtained as

$$n_s = \int f_s\, \mathrm{d}^3 p, \tag{5}$$

$$\boldsymbol{j}_s = e_s \int \boldsymbol{v} f_s\, \mathrm{d}^3 p, \tag{6}$$

where $\boldsymbol{v} = [\boldsymbol{p} - (e_s/c)\boldsymbol{A}]/m_s$. The electromagnetic fields, $\boldsymbol{E}$ and $\boldsymbol{B}$, are determined by substituting n_s and $\boldsymbol{j}_s$ to the Maxwell equations,

$$\nabla \times \boldsymbol{E} = -\frac{1}{c}\frac{\partial \boldsymbol{B}}{\partial t}, \tag{7}$$

$$\nabla \times \boldsymbol{B} = \frac{4\pi}{c}\sum_s \boldsymbol{j}_s + \frac{1}{c}\frac{\partial \boldsymbol{E}}{\partial t}, \tag{8}$$

$$\nabla \cdot \boldsymbol{E} = 4\pi \sum_s e_s n_s, \tag{9}$$

$$\nabla \cdot \boldsymbol{B} = 0. \tag{10}$$

The Vlasov–Maxwell system, equations (4)–(10), gives a basic description of a high temperature collisionless plasma.

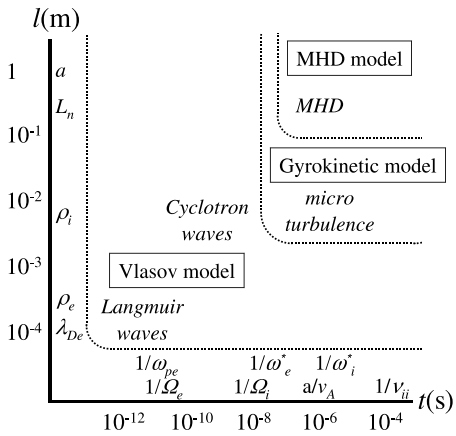

Figure 1. Enormous ranges of spatio-temporal scales in a fusion plasma and applicability of Vlasov, gyrokinetic and MHD models. Here, ω_{ps} is the plasma oscillation frequency, Ω_s is the cyclotron frequency, ω_s^* is the diamagnetic rotation frequency, v_{A} is the Alfvén velocity, ν_{ii} is the ion–ion collision frequency, $\lambda_{\mathrm{D}s}$ is the Debye length, ρ_s is the Larmor radius, L_n is the scale length of the equilibrium density profile, a is the plasma size and s denotes the particle species.

2.2. The gyrokinetic model

Although the Vlasov–Maxwell system is a reduced kinetic description compared with the Newton–Maxwell system, it involves enormous ranges of spatio-temporal scales as shown in figure 1. Therefore, it is still difficult to simulate low frequency phenomena such as microturbulence and MHD waves via the Vlasov–Maxwell system. To avoid a direct

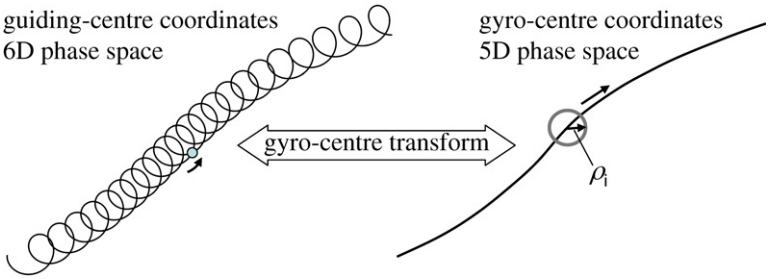

Figure 2. By applying the gyro-centre transform, fast gyro-motion is eliminated, and the problem is reduced from 6D to 5D while keeping kinetic effects such as the finite Larmor radius effect.

treatment of a multiple hierarchy of spatio-temporal scales, a nonlinear gyrokinetic model [7, 8] has been developed by eliminating high-frequency phenomena with $\omega > \Omega_s$ while keeping essential kinetic effects, where $\Omega_s = (e_s B_0)/(m_s c)$ is the cyclotron frequency. While earlier gyrokinetic equations were formulated by gyro-averaging the Vlasov equation based on the recursive method [7], the modern gyrokinetic theory [5] consists of the guiding-centre transform [9–12] and the gyro-centre transform [13–16], which are based on the Hamiltonian or Lagrangian formalism with the Lie perturbation theory [17, 18]. The latter approach enables a rigorous treatment of collisionless turbulent dynamics while keeping the first principles such as the symmetry and conservation properties, which are important physics ingredients for describing the underlying physics and are useful for a nonlinear simulation. In this section, we review the gyrokinetic Vlasov–Maxwell equations, which are valid up to $\mathcal{O}(\epsilon_g)$, without strong equilibrium flows, where ϵ_g is a smallness parameter in the gyrokinetic ordering. This approximation is widely used for gyrokinetic simulations of core plasmas with subsonic flows. In analysing core and edge plasmas with strong flows, extended gyrokinetic models in the presence of toroidal rotation [19], static $\boldsymbol{E}_r \times \boldsymbol{B}$ flows [19–21] and dynamic $\boldsymbol{E}_r \times \boldsymbol{B}$ flows [22–24] were proposed. An extension of gyrokinetic equations including mean flows was also addressed based on the recursive method [25, 26].

From experimental observations in core plasmas with subsonic flows, tokamak microturbulence is considered to obey the gyrokinetic ordering in ϵ_g,

$$\frac{\omega}{\Omega_s} \sim \frac{k_\parallel}{k_\perp} \sim \frac{v_E}{v_{ts}} \sim \frac{\delta n_s}{n_0} \sim \frac{B_1}{B_0} \sim \frac{\rho_s}{L_n} \sim \mathcal{O}(\epsilon_g), \tag{11}$$

where ω is a characteristic frequency of microturbulence, $\boldsymbol{B}_0 = \nabla \times \boldsymbol{A}_0$ is the equilibrium field, $\boldsymbol{B}_1 = \nabla \times \boldsymbol{A}_1$ is the perturbed field, $\boldsymbol{b} = \boldsymbol{B}_0/B_0$ is the unit vector in the direction of $\boldsymbol{B}_0$, $k_\parallel = \boldsymbol{k} \cdot \boldsymbol{b}$ and $k_\perp = |\boldsymbol{k} \times \boldsymbol{b}|$ are parallel and perpendicular components of the wave vector $\boldsymbol{k}$, v_E is the *perturbed* $\boldsymbol{E} \times \boldsymbol{B}$ drift velocity, v_{ts} is the thermal velocity, n_0 is the equilibrium density, δn_s is the perturbed density, $\rho_s = v_\perp/\Omega_s$ is the Larmor radius, $L_n = |\nabla \ln n_0|^{-1}$ is a characteristic scale length of n_0. Here, $v_E/v_{ts} \sim \mathcal{O}(\epsilon_g)$ leads to $e_s\phi/T_s \sim \mathcal{O}(\epsilon_g)$ for microscopic fields with $k_\perp \rho_s \sim \mathcal{O}(1)$, while $e_s\phi/T_s \sim \mathcal{O}(1)$ is expected for macroscopic fields with $k_\perp L_n \sim \mathcal{O}(1)$, where T_s is the temperature. For a fusion plasma with finite but small β (typically $\beta \sim 1\%$), the perturbed field is given as $\boldsymbol{B}_1 = \nabla \times A_\parallel \boldsymbol{b}$, and the parallel component of $\boldsymbol{B}_1$ is often neglected compared with $\boldsymbol{B}_0$, where $\beta = (n_0 T_i + n_0 T_e)/(B_0^2/8\pi)$ is the ratio of the plasma kinetic pressure to the magnetic pressure. As shown in figure 2, the single particle motion under strong ambient magnetic fields consists of the superposition of a fast periodic gyro-motion and a slow guiding-centre motion. Low frequency perturbations satisfying this ordering mainly affect the latter motion, and the magnetic moment, $\mu = m_s v_\perp^2/2B_0$, becomes an approximate adiabatic invariant. Although the gyrokinetic equation in the canonical guiding-centre coordinates [27] may be useful in linear stability analyses, for the purpose of a gyrokinetic simulation, it is convenient to use the non-canonical guiding-centre coordinates $\boldsymbol{Z}_{GC} = (t; \boldsymbol{R}, u, \mu, \xi)$, where approximate configuration space variables $\boldsymbol{R}$ are separated from velocity-space variables. Here, $\boldsymbol{R} = \boldsymbol{q} - \rho$ is the guiding-centre position, $\rho = \boldsymbol{b} \times \boldsymbol{v}/\Omega_s$ is the gyroradius vector, $u = v_\parallel + (e_s/cm_s)A_\parallel$ is the generalized parallel velocity, $v_\parallel = \boldsymbol{v} \cdot \boldsymbol{b}$ and $v_\perp = |\boldsymbol{v} \times \boldsymbol{b}|$ are parallel and perpendicular components of the velocity, respectively, $\xi = \tan^{-1}(\boldsymbol{v}\cdot\boldsymbol{e}_1/\boldsymbol{v}\cdot\boldsymbol{e}_2)$ is the gyro-phase angle and $\boldsymbol{e}_1$ and $\boldsymbol{e}_2$ are orthogonal unit vectors defined as $\boldsymbol{e}_1 \times \boldsymbol{e}_2 = \boldsymbol{b}$. The guiding-centre transform is given by a near identity transformation using the Lie transform method for non-canonical variables, and fast action-angle variables of unperturbed particle orbits (μ, ξ) are decoupled from 6D phase space coordinates. Although the transformation is systematically calculated up to arbitrary order in $\epsilon_B = \rho_s/L_B$ while keeping the Hamiltonian structure of unperturbed particle orbits, a gyrokinetic simulation normally uses its leading order expression. Here, $L_B = |\nabla \ln B_0|^{-1}$ is a characteristic scale length of the equilibrium magnetic field. In the guiding-centre coordinates, the perturbed Hamiltonian is written as

$$\begin{aligned} H_s &= \tfrac{1}{2} m_s \left| u - \frac{e_s}{cm_s} A_\parallel \right|^2 + \mu B_0 + e_s \phi, \\ &= \tfrac{1}{2} m_s u^2 + \mu B_0 + e_s \Psi + \mathcal{O}(\epsilon_g^2), \end{aligned} \tag{12}$$

where $\Psi(\boldsymbol{R}, u, \mu, \xi, t) = \phi - uA_\parallel/c$ is the generalized potential. In equation (12), the Coulomb gauge is used and $A_\perp$ or the parallel magnetic perturbation is neglected.

We then separate a fast gyro-phase dependent part of the perturbation from the perturbed Hamiltonian (12) by applying the gyro-centre transform, and find new coordinates, the gyro-centre coordinates $\boldsymbol{Z}_{GY} = (t; \bar{\boldsymbol{R}}, \bar{u}, \bar{\mu}, \bar{\xi})$, where an approximate invariant μ in the presence of low frequency perturbations becomes an exact invariant $\bar{\mu}$ and its conjugate variable $\bar{\xi}$ is seen as an ignorable coordinate. The gyro-centre transform valid up to $\mathcal{O}(\epsilon_g)$ is given as

$$\boldsymbol{Z}_{GY} = \boldsymbol{Z}_{GC} + \{\tilde{S}, \boldsymbol{Z}_{GC}\} + \mathcal{O}(\epsilon_g^2), \tag{13}$$

where $\{\cdot,\cdot\}$ is the Poisson bracket in the gyro-centre coordinates,

$$\{F,G\} \equiv \frac{\Omega_s}{B_0}\left(\frac{\partial F}{\partial \xi}\frac{\partial G}{\partial \mu} - \frac{\partial F}{\partial \mu}\frac{\partial G}{\partial \xi}\right) + \frac{\boldsymbol{B}^*}{m_s B_\parallel^*}\cdot\left(\nabla F\frac{\partial G}{\partial u} - \frac{\partial F}{\partial u}\nabla G\right) - \frac{c}{e_s B_\parallel^*}\boldsymbol{b}\cdot\nabla F\times\nabla G, \tag{14}$$

and $B_\parallel^* = \boldsymbol{b}\cdot\boldsymbol{B}^*$ is a parallel component of $\boldsymbol{B}^*(Z_{\rm GC}) = \boldsymbol{B}_0 + (B_0\bar{u}/\Omega_s)\nabla\times\boldsymbol{b}$. The generating function $\tilde{S}$ is solved as

$$\tilde{S}(\boldsymbol{Z}_{\rm GC},t) = \frac{e_s}{\Omega_s}\int^{\xi}\left[\Psi - \langle\Psi\rangle_\xi\right]\mathrm{d}\xi', \tag{15}$$

where the gyro-average is defined as $\langle\cdot\rangle_\xi \equiv \oint\cdot\mathrm{d}\xi/2\pi$. This transform is formulated based on the Lie-transform perturbation theory, so that the transform keeps the area preserving property of the Hamiltonian system up to arbitrary order in $\epsilon_{\rm g}$ and the Poisson bracket becomes form invariant. After the transform, ξ-dependent non-secular perturbations are absorbed in the generating function $\tilde{S}$, and the Hamiltonian $\bar{H}_s$ becomes independent of $\bar{\xi}$,

$$\bar{H}_s = \tfrac{1}{2}m_s\bar{u}^2 + \bar{\mu}B_0 + e_s\langle\Psi\rangle_{\bar{\xi}}. \tag{16}$$

It is noted that among several different choices of independent variables, especially in the electromagnetic case, in this section, we have chosen to use the generalized parallel velocity, which is transformed as $\bar{u} = u + \{\tilde{S},u\} + \mathcal{O}(\epsilon_{\rm g}^2)$ [28]. In this choice, functional forms of the Hamiltonian (12) and the Poisson bracket (14) become the same as those in the electrostatic limit, and we can easily find the electromagnetic gyro-centre transform by replacing ϕ with Ψ in the electrostatic gyro-centre transform.

We then have a reduced kinetic equation or a gyrokinetic equation, which describes the evolution of the particle distribution function expressed in gyro-centre coordinates $\bar{f}_s$ in 5D phase space,

$$\begin{aligned}\frac{\mathrm{D}\bar{f}_s}{\mathrm{D}t} &\equiv \frac{\partial\bar{f}_s}{\partial t} + \left\{\bar{f}_s,\bar{H}_s\right\}\\ &= \frac{\partial\bar{f}_s}{\partial t} + \frac{\mathrm{d}\bar{\boldsymbol{R}}}{\mathrm{d}t}\cdot\frac{\partial\bar{f}_s}{\partial\bar{\boldsymbol{R}}} + \frac{\mathrm{d}\bar{u}}{\mathrm{d}t}\frac{\partial\bar{f}_s}{\partial\bar{u}},\\ &= 0,\end{aligned} \tag{17}$$

where the nonlinear characteristics, $\dot{\boldsymbol{Z}}_{\rm GY} = \{\boldsymbol{Z}_{\rm GY},\bar{H}\}$, are given as

$$\begin{aligned}\frac{\mathrm{d}\bar{\boldsymbol{R}}}{\mathrm{d}t} &= \frac{\boldsymbol{B}^*}{m_s B_\parallel^*}\frac{\partial\bar{H}_s}{\partial\bar{u}} + \frac{c}{e_s B_\parallel^*}\boldsymbol{b}\times\nabla\bar{H}_s\\ &= \bar{u}\boldsymbol{b} - \frac{e_s}{cm_s}\langle A_\parallel\rangle_{\bar{\xi}}\frac{\boldsymbol{B}^*}{B_\parallel^*}\\ &\quad + \frac{c}{e_s B_\parallel^*}\boldsymbol{b}\times\left(e_s\nabla\langle\Psi\rangle_{\bar{\xi}} + m_s\bar{u}^2\boldsymbol{b}\cdot\nabla\boldsymbol{b} + \bar{\mu}\nabla B_0\right),\end{aligned} \tag{18}$$

$$\begin{aligned}\frac{\mathrm{d}\bar{u}}{\mathrm{d}t} &= -\frac{\boldsymbol{B}^*}{m_s B_\parallel^*}\cdot\nabla\bar{H}_s\\ &= -\frac{\boldsymbol{B}^*}{m_s B_\parallel^*}\cdot\left(e_s\nabla\langle\Psi\rangle_{\bar{\xi}} + \bar{\mu}\nabla B_0\right),\end{aligned} \tag{19}$$

$$\frac{\mathrm{d}\bar{\mu}}{\mathrm{d}t} = 0. \tag{20}$$

Since the gyrokinetic equation (17) is the Liouville equation, $\bar{f}_s$ is conserved along the nonlinear characteristics. This leads to the conservation of an arbitrary function of $\bar{f}_s$. Another important property is the phase space conservation,

$$\nabla\cdot\left(\mathcal{J}_s\frac{\mathrm{d}\bar{\boldsymbol{R}}}{\mathrm{d}t}\right) + \frac{\partial}{\partial\bar{u}}\left(\mathcal{J}_s\frac{\mathrm{d}\bar{u}}{\mathrm{d}t}\right) = 0, \tag{21}$$

where $\mathcal{J}_s = m^2B_\parallel^*$ is the Jacobian of the gyro-centre coordinates. From this property, the gyrokinetic equation (17) can also be written in a conservative form

$$\frac{\partial\mathcal{J}_s\bar{f}_s}{\partial t} + \nabla\cdot\left(\mathcal{J}_s\frac{\mathrm{d}\bar{\boldsymbol{R}}}{\mathrm{d}t}\bar{f}_s\right) + \frac{\partial}{\partial\bar{u}}\left(\mathcal{J}_s\frac{\mathrm{d}\bar{u}}{\mathrm{d}t}\bar{f}_s\right) = 0. \tag{22}$$

The guiding-centre orbit (18) is determined by the parallel motion and the perpendicular drift motion associated with the electromagnetic perturbation and the curvature and gradient of the magnetic field. In equation (19), the generalized parallel velocity suffers from acceleration forces associated with the electromagnetic perturbation and the gradient of the magnetic field. The latter force works as the magnetic mirror in the presence of two constants of motion in the unperturbed orbit, the energy $\varepsilon = m_s\bar{u}^2/2 + \bar{\mu}B_0$ and the magnetic moment $\bar{\mu}$. In figure 3, the unperturbed orbits in a tokamak configuration show complicated trajectories depending on the pitch angle $\zeta = \sin^{-1}(v_\perp/v)$ at the outboard mid-plane, and are classified mainly into passing and trapped particles. While passing particles are characterized by the parallel motion and the perpendicular magnetic drift, trapped particles follow a bounce motion in the weak field side, and their magnetic drift results in a toroidal precession motion. It is noted that in a treatment of the bounce motion, in cases where it is fast compared with other scales of interest, a similar approach as in gyrokinetics can be applied to formulate the bounce-averaged kinetic equation [29, 30]. Projected onto the poloidal plane, unperturbed particle orbits are closed, which correspond to constant surfaces of the canonical toroidal angular momentum, p_φ, which is another constant of motion in the axisymmetric tokamak configuration. Therefore, the equilibrium solution of the collisionless gyrokinetic equation (17) is given as a function of three constants of motion, $f_{\rm Cs}(p_\varphi,\varepsilon,\bar{\mu})$, where p_φ is an approximate flux label in the canonical coordinates. It is noted that in non-axisymmetric configurations such as 3D helical systems and tokamaks with magnetic field ripple, p_φ is not a constant of motion and the projected orbits of ripple-trapped particles are not closed. The parallel and perpendicular motion in the guiding-centre orbit is closely related to microinstabilities, which are excited by the density gradient, the ion temperature gradient (ITG) and the electron temperature gradient (ETG) through various wave–particle resonant interactions. Depending on the resonance condition, microinstabilities are classified into slab modes, toroidal modes and trapped particle modes, where the parallel motion of passing particles, the magnetic drift of passing particles and the toroidal precession of trapped particles are essential for the wave–particle interaction, respectively. Detailed classification of micro-instabilities can be found in the literature [31–34] (also see section 4.1). On the other hand, these wave–particle interactions also work as a damping mechanism for smaller scale perturbations. In particular, high-$k_\parallel$ components suffer

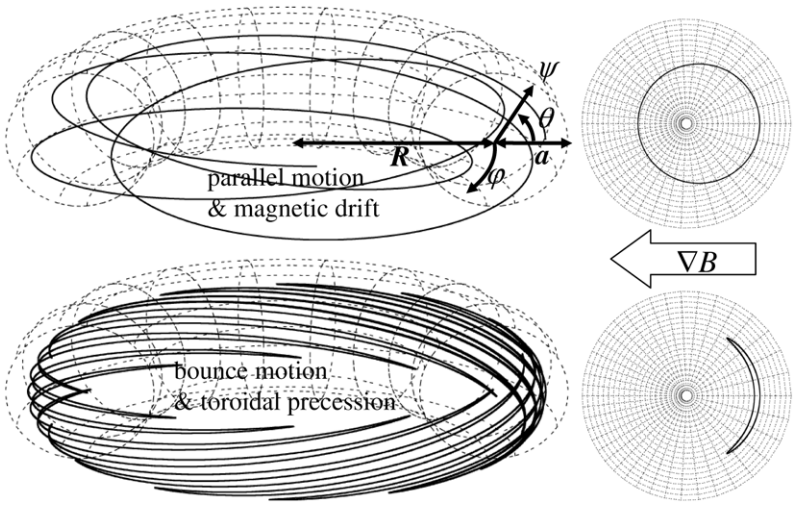

Figure 3. Typical unperturbed guiding-centre orbits of passing and trapped particles in a tokamak configuration, and their projection on the poloidal cross-section. The coordinates (ψ, θ, φ) show the radial direction, the poloidal angle and the toroidal angle.

from Landau damping due to the parallel motion of passing particles, which restricts turbulent structures to so-called flute-like structures with $k_\parallel \rho_s \ll 1$.

Finally, the equation system is closed by the Poisson–Ampère laws. The pull back transform from the gyro-centre distribution $\bar{f}_s$ to the guiding-centre distribution $\hat{f}_s$ is given as

$$\begin{aligned}\hat{f}_s &= \bar{f}_s + \{\tilde{S}, \bar{f}_s\} + \mathcal{O}\left(\epsilon_g^2\right) \\ &\simeq \bar{f}_s + \{\tilde{S}, f_{Ms}\} + \mathcal{O}\left(\epsilon_g^2\right), \end{aligned} \tag{23}$$

where f_{Ms} is a local Maxwellian distribution defined at each flux surface, and the second relation is obtained because $\delta \bar{f}_s = \bar{f}_s - f_{Ms}$ is small compared with f_{Ms} or $\delta \bar{f}_s / f_{Ms} \sim \mathcal{O}(\epsilon_g)$. The particle density n_s and the parallel current density j_s are, respectively, calculated as

$$\begin{aligned} n_s &= \int \hat{f}_s(\boldsymbol{Z}) \delta\left([\boldsymbol{R} + \rho_s] - \boldsymbol{x}\right) \mathcal{J}_s \mathrm{d}^6 Z \\ &= \int \left[\bar{f}_s + \frac{\Omega_s}{B_0} \frac{\partial \tilde{S}}{\partial \xi} \frac{\partial f_{Ms}}{\partial \mu} \right] \delta\left([\boldsymbol{R} + \rho_s] - \boldsymbol{x}\right) \mathcal{J}_s \mathrm{d}^6 Z + \mathcal{O}(\epsilon_g^2) \\ &= \int \bar{f}_s \delta\left([\boldsymbol{R} + \rho_s] - \boldsymbol{x}\right) \mathcal{J}_s \mathrm{d}^6 Z - \frac{e_s n_0}{T_s} \left(\phi - \langle \bar{\phi} \rangle_\xi\right), \end{aligned} \tag{24}$$

$$\begin{aligned} j_s &= e_s \int v_\parallel \hat{f}_s(\boldsymbol{Z}) \delta\left([\boldsymbol{R} + \rho_s] - \boldsymbol{x}\right) \mathcal{J}_s \mathrm{d}^6 Z \\ &= e_s \int \left[u \bar{f}_s - \frac{e_s}{c m_s} A_\parallel \bar{f}_{Ms} + u \frac{\Omega_s}{B_0} \frac{\partial \tilde{S}}{\partial \xi} \frac{\partial f_{Ms}}{\partial \mu} \right] \\ &\quad \times \delta\left([\boldsymbol{R} + \rho_s] - \boldsymbol{x}\right) \mathcal{J}_s \mathrm{d}^6 Z + \mathcal{O}(\epsilon_g^2) \\ &= e_s \int u \bar{f}_s \delta\left([\boldsymbol{R} + \rho_s] - \boldsymbol{x}\right) \mathcal{J}_s \mathrm{d}^6 Z - \frac{e_s n_0}{c m_s} \langle \bar{A}_\parallel \rangle_\xi. \end{aligned} \tag{25}$$

Here, the second term in the rhs of equation (24) shows the polarization density due to the finite Larmor radius (FLR) effect. In equation (25), a part of the magnetization current (the third term in the second equation) is cancelled with the second term in the second equation, which appears due to the use of u.

By substituting equations (24) and (25), the Maxwell equations yield the gyrokinetic Poisson–Ampère laws,

$$\begin{aligned} -\nabla^2 \phi &= 4\pi \sum_s e_s n_s, \\ &= \sum_s \left[4\pi e_s \int \delta \bar{f}_s \delta([\bar{\boldsymbol{R}} + \bar{\rho}_s] - \boldsymbol{x}) \mathcal{J}_s \mathrm{d}^6 \bar{Z} \right. \\ &\quad \left. - \frac{1}{\lambda_{Ds}^2} \left(\phi - \langle \bar{\phi} \rangle_\xi\right) \right], \end{aligned} \tag{26}$$

$$\begin{aligned} -\nabla_\perp^2 A_\parallel &= \frac{4\pi}{c} \sum_s j_s \\ &= \sum_s \left[\frac{4\pi e_s}{c} \int \bar{u} \delta \bar{f}_s \delta([\bar{\boldsymbol{R}} + \bar{\rho}_s] - \boldsymbol{x}) \mathcal{J}_s \mathrm{d}^6 \bar{Z} \right. \\ &\quad \left. - \frac{\omega_{ps}^2}{c^2} \langle \bar{A}_\parallel \rangle_\xi \right], \end{aligned} \tag{27}$$

where λ_{Ds} is the Debye length, ω_{ps} is the plasma oscillation frequency, and $\langle \bar{\cdot} \rangle_\xi = \int \langle \cdot \rangle_\xi f_{Ms} \delta([\bar{\boldsymbol{R}} + \bar{\rho}_s] - \boldsymbol{x}) \mathcal{J}_s \mathrm{d}^6 \bar{Z} / n_0$. The displacement current in equation (8) is neglected for low frequency phenomena considered here. In deriving equations (26) and (27), nonlinear polarization and magnetization effects, which are higher order in ϵ_g, and other higher order terms are neglected, and final equations are given in rather simple forms which are suitable for numerical implementation. The gyrokinetic Vlasov–Maxwell system, equations (17), (26) and (27), is a standard kinetic model to describe micro-turbulence in the plasma core.

The most important feature of the gyrokinetic Vlasov–Maxwell system is that high-frequency phenomena such as the Langmuir wave and the cyclotron wave are eliminated while keeping essential kinetic effects for low frequency microturbulence. From the viewpoint of the simulation, the limitations on the time step and the grid spacing are relaxed from $\Delta t \omega_{ps} < 1$ and $\Delta r < \lambda_{Ds}$ to $\Delta t \omega_s^* < 1$ and $\Delta r < \rho_s$, and the computational cost is dramatically reduced, where ω_s^* is the diamagnetic rotation frequency. Another important feature is the conservation properties. Since the transform is designed to keep the Hamiltonian structure of the system,

the gyrokinetic Vlasov–Maxwell system conserves the particle number, momentum, energy and entropy as in the Vlasov–Maxwell system. By calculating a relation, $\int \bar{H}_s \partial_t \bar{f}_s \mathcal{J}_s \mathrm{d}^6 Z = -\int \{\bar{H}_s \bar{f}_s, \bar{H}_s\} \mathcal{J}_s \mathrm{d}^6 Z = 0$ [35], equations (17), (26) and (27) yield the total energy conservation,

$$\sum_s \int \bar{H}_s \frac{\partial \bar{f}_s}{\partial t} \mathcal{J}_s \mathrm{d}^6 \bar{Z} = \frac{\mathrm{d}}{\mathrm{d}t} \left(E_k + E_\phi + E_{A_\parallel} \right) = 0, \tag{28}$$

$$E_k = \sum_s \left[\int \left(\tfrac{1}{2} m_s \bar{u}^2 + \bar{\mu} B_0 \right) \bar{f}_s \mathcal{J}_s \mathrm{d}^6 \bar{Z} \right], \tag{29}$$

$$E_\phi = \frac{1}{8\pi} \int |\nabla \phi|^2 \mathrm{d}^3 x + \frac{1}{8\pi} \sum_s \sum_{\boldsymbol{k}} \frac{1}{\lambda_{\mathrm{D}s}^2} \left[1 - \Gamma_0 (k_\perp^2 \rho_{\mathrm{ts}}^2) \right] |\phi_{\boldsymbol{k}}|^2, \tag{30}$$

$$E_{A_\parallel} = \frac{1}{8\pi} \int |\nabla_\perp A_\parallel|^2 \mathrm{d}^3 x + \frac{1}{8\pi} \sum_s \sum_{\boldsymbol{k}} \frac{\omega_{\mathrm{ps}}^2}{c^2} \Gamma_0 (k_\perp^2 \rho_{\mathrm{ts}}^2) |A_{\parallel \boldsymbol{k}}|^2, \tag{31}$$

where $\phi = \sum_{\boldsymbol{k}} \phi_{\boldsymbol{k}} \exp(\mathrm{i}\boldsymbol{k} \cdot \boldsymbol{x})$, ρ_{ts} is the Larmor radius estimated with the thermal velocity, $A_\parallel = \sum_{\boldsymbol{k}} A_{\parallel \boldsymbol{k}} \exp(\mathrm{i}\boldsymbol{k} \cdot \boldsymbol{x})$, $\Gamma_0(b) = I_0(b) \mathrm{e}^{-b}$ and I_0 is the zeroth order modified Bessel function. Although the energy conservation (28) is derived straightforwardly for the present gyrokinetic Vlasov–Maxwell equations with linear polarization and magnetization effects, in general, it is difficult to find an exact energy conservation when higher order nonlinear polarization and magnetization effects are retained. In higher order gyrokinetics, the gyrokinetic field theory with Lagrangian or Eulerian approaches [28, 36] was developed to formulate the gyrokinetic Vlasov–Maxwell equations where an exact energy conservation law is demonstrated based on Noether's theorem. An exact conservation property is important especially in studying nonlinear problems, where an analytic solution can hardly be found. The conservation of particles and energy is normally checked as a stringent test of the quality of the nonlinear simulation.

2.3. Extensions of gyrokinetic model for simulations

Although the gyrokinetic Vlasov–Maxwell system, equations (17), (26) and (27), gives a clear physics foundation for studying low frequency phenomena in the collisionless limit, one would often like to include collisional effects for practical simulations, as collisions are often experimentally relevant and even weak collisions can sometimes be important for the following reasons. Firstly, the gyrokinetic equation (17) continuously produces fine scale velocity-space structures due to linear and nonlinear mixing effects. From the viewpoint of the entropy balance relation [37–39], such a collisionless system does not formally reach a statistically steady state in all possible quantities when turbulent transport is at a finite level [40]. If we consider stretching due to the parallel streaming, the ballistic mode leads to fine scale structures in $v_\parallel$, which, in a collisionless system, will inevitably exceed the maximum numerical resolution. In order to smear out such structures, we need physical or numerical dissipation mechanisms both in the pitch angle ζ and in the energy ε. Secondly, a collisionless gyrokinetic Vlasov equilibrium $f_{\mathrm{C}s}(p_\varphi, \varepsilon, \bar{\mu})$ does not satisfy the quasi-neutrality condition without equilibrium electric fields, because constant p_φ surfaces or particle orbit widths are different depending on the particle species s. This means that a relevant kinetic equilibrium naturally involves electric fields, which are subject to the force balance relation involving the neoclassical viscosity [41, 42]. The neoclassical physics strongly influences the parallel flow dynamics and the bootstrap current, while the poloidal rotation sometimes deviates from the neoclassical theory prediction. The bootstrap current is an essential ingredient in advanced magnetic fusion experiments. In addition, the neoclassical perpendicular transport gives a baseline of transport levels, when turbulent transport is quenched, e.g., in transport barriers. Thirdly, collisions are considered to play important roles also in the turbulent transport. Ion–ion collisions enhance the damping of zonal flows, which may lead to an increase in ion heat transport near a nonlinear threshold [43, 44], and electron–ion collisions affect the trapped electron mode (TEM) by effective reduction in trapped electron drive [45]. For these reasons, we need physically relevant collisional dissipation even in simulating high temperature fusion plasmas. A collision model for a weakly coupled plasma is given by the Fokker–Planck collision operator [46],

$$C(f_{s'}, f_s) = \sum_{s'} -\frac{\partial}{\partial \boldsymbol{v}} \cdot \left(\left\langle \frac{\Delta \boldsymbol{v}}{\Delta t} \right\rangle f_s \right) + \frac{1}{2} \frac{\partial^2}{\partial \boldsymbol{v} \partial \boldsymbol{v}} : \left(\left\langle \frac{\Delta \boldsymbol{v} \Delta \boldsymbol{v}}{\Delta t} \right\rangle f_s \right), \tag{32}$$

$$\left\langle \frac{\Delta \boldsymbol{v}}{\Delta t} \right\rangle = \gamma_{ss'} \frac{\partial}{\partial \boldsymbol{v}} \mathcal{H}_{s'}(\boldsymbol{v}), \tag{33}$$

$$\left\langle \frac{\Delta \boldsymbol{v} \Delta \boldsymbol{v}}{\Delta t} \right\rangle = \gamma_{ss'} \frac{\partial^2}{\partial \boldsymbol{v} \partial \boldsymbol{v}} \mathcal{G}_{s'}(\boldsymbol{v}), \tag{34}$$

where $\gamma_{ss'} = (4\pi e_s^2 e_{s'}^2 / m_s^2) \ln \Lambda$, $\ln \Lambda$ is the Coulomb logarithm, and the Rosenbluth potentials, $\mathcal{H}_{s'}$ and $\mathcal{G}_{s'}$, are given as

$$\mathcal{H}_{s'}(\boldsymbol{v}) = \left(1 + \frac{m_s}{m_{s'}} \right) \int \frac{f_{s'}(\boldsymbol{v}')}{|\boldsymbol{v} - \boldsymbol{v}'|} \mathrm{d}^3 v', \tag{35}$$

$$\mathcal{G}_{s'}(\boldsymbol{v}) = \int f_{s'}(\boldsymbol{v}') |\boldsymbol{v} - \boldsymbol{v}'| \, \mathrm{d}^3 v'. \tag{36}$$

Basic properties of the Fokker–Planck collision operator are the conservation of the particle number, the momentum and the energy, the annihilation of a shifted Maxwellian distribution, and Boltzmann's H-theorem, which are physical constraints used also in developing its reduced models. In studying core plasmas, which are expected to be close to a local thermodynamic equilibrium or a Maxwellian distribution, the operator can be further simplified to its linear version,

$$C(f_s) = \sum_{s'} -\frac{\partial}{\partial \boldsymbol{v}} \cdot \left(\left\langle \frac{\Delta \boldsymbol{v}}{\Delta t} \right\rangle_0 f_s \right) + \frac{1}{2} \frac{\partial^2}{\partial \boldsymbol{v} \partial \boldsymbol{v}} : \left(\left\langle \frac{\Delta \boldsymbol{v} \Delta \boldsymbol{v}}{\Delta t} \right\rangle_0 f_s \right) + P_{s'} f_{\mathrm{M}s}, \tag{37}$$

where $\langle \Delta \boldsymbol{v} / \Delta t \rangle_0$ and $\langle \Delta \boldsymbol{v} \Delta \boldsymbol{v} / \Delta t \rangle_0$ are evaluated using a Maxwellian field particle distribution $f_{\mathrm{M}s'}$, and a field particle operator $P_{s'} f_{\mathrm{M}s}$ is determined by the conservation of momentum and energy [47]. In calculating neoclassical transport coefficients, the yet simpler Lorentz type collision operator consisting of pitch angle scattering and a momentum

restoring term is often used as a good approximation [41, 42]. A similar reduced collision operator with $v_\parallel$ scattering was proposed as a minimum model to recover the neoclassical physics for the purpose of a gyrokinetic simulation, which often uses $v_\parallel$ and μ as velocity-space coordinates [48]. Since the collisional dissipation violates the Hamiltonian structure of the problem, we cannot construct the gyro-centre transform including collisions. Therefore, after applying the guiding-centre transform to obtain a guiding-centre collision operator, we find its gyro-phase independent form using a multiple time-scale expansion in $\epsilon_\nu = \nu_{ss}/\Omega_s$ and gyro-averaging procedures [49], and add it to the rhs of the gyrokinetic equation (17). A general form of a gyro-centre collision operator $C_{\rm GY}$ to lowest order in ϵ_B, $\epsilon_{\rm g}$ may be written as [49–52]

$$C_{\rm GY}(\bar{f}_s) = \sum_{\boldsymbol{k}} \mathrm{e}^{\mathrm{i}\boldsymbol{k}\cdot\bar{\boldsymbol{R}}} \left\langle \mathrm{e}^{\mathrm{i}\boldsymbol{k}\cdot\rho_s} C\left(\mathrm{e}^{-\mathrm{i}\boldsymbol{k}\cdot\rho_s}\left[\bar{f}_{s\boldsymbol{k}} + \{\tilde{S}, f_{\mathrm{M}s}\}_{\boldsymbol{k}}\right]\right)\right\rangle_{\bar{\xi}}. \tag{38}$$

The FLR correction in equation (38) leads to spatial diffusion in $\bar{\boldsymbol{R}}$, which may be significant for short wavelength perturbations with $k_\perp\rho_s \geqslant 1$. Since the operator becomes non-local, conservation properties of the collision operator are complicated. However, when we simulate the neoclassical physics in the presence of relatively long wavelength perturbations with $k_\perp\rho_s < 1$, its drift-kinetic limit, $C_{\rm GY}(\bar{f}_s) = C(\bar{f}_s)$, may be a good approximation as in most neoclassical simulations.

In the axisymmetric limit with macroscopic radial electric fields, the gyrokinetic equation naturally converges to the drift-kinetic equation which is a physical model used in the neoclassical theory [41, 42]. Therefore, collisional gyrokinetic simulations are expected to recover the neoclassical transport. The radial electric field can be determined by the gyrokinetic Poisson equation (26), which reproduces geodesic acoustic mode oscillations in the axisymmetric limit (see section 4.2.2). By taking the time derivative and the flux-surface average, equation (26) yields the equation for the radial electric field, which was used to determine the neoclassical radial electric field [53, 54],

$$\left\langle \frac{\rho_{\rm ti}^2}{\lambda_{\rm Di}^2}|\nabla\psi|^2\right\rangle_{\rm f} \frac{\partial^2\langle\phi\rangle_{\rm f}}{\partial t\partial\psi} = 4\pi\sum_s \left\langle e_s \int \delta\bar{f}_s\,(\boldsymbol{v}_B\cdot\nabla\psi)\,\mathcal{J}_s\,\mathrm{d}\bar{u}\,\mathrm{d}\bar{\mu}\,\mathrm{d}\bar{\xi}\right\rangle_{\rm f}, \tag{39}$$

where ψ is the equilibrium magnetic poloidal flux, $\langle\cdot\rangle_{\rm f}$ denotes the flux-surface average, $\boldsymbol{v}_B$ is magnetic drift term in equation (18). In a quasi-steady state, equation (39) leads to ambipolar particle transport, which is consistent with the lowest order neoclassical theory and the radial electric field is determined to satisfy the force balance relation [41, 42],

$$\langle U_\parallel\rangle_{\rm f} = \frac{T_{\rm i}I}{m_{\rm i}\Omega_{\rm i}}\left[(k-1)\frac{\mathrm{d}\ln T_{\rm i}}{\mathrm{d}\psi} - \frac{\mathrm{d}\ln n_{\rm i}}{\mathrm{d}\psi} - \frac{e}{T_{\rm i}}\frac{\partial\langle\phi\rangle_{\rm f}}{\mathrm{d}\psi}\right], \tag{40}$$

where $U_\parallel$ is the parallel flow, $I = RB_\varphi$, R is the major radius, B_φ is the toroidal magnetic field and k is a coefficient depending on the ion collisionality. In fact, recent collisional gyrokinetic simulations [55–58] recovered this relation as well as neoclassical ion heat transport in the axisymmetric limit. It is noted that when a parallel flow profile is given, equation (40) dictates the radial electric field, because it is adjusted on a fast time scale compared with collisional momentum transport. However, in [59], it was shown that the parallel flow itself (and the corresponding radial electric field) cannot be determined by the lowest order neoclassical theory, and that to estimate the parallel flow within the framework of the neoclassical theory, one needs to calculate the conservation of angular momentum up to higher order. It is noted that this argument does not apply to non-axisymmetric configurations, where the lowest order neoclassical particle transport is not ambipolar. In [60], it was pointed out that higher order gyrokinetic theory is needed to determine the radial electric field consistent with the neoclassical toroidal viscosity. However, in turbulent tokamaks, parallel flow or toroidal rotation may be dominated by the balance between turbulent momentum transport (see section 5.1.4) and external torque, which are normally larger than the neoclassical momentum transport. Therefore, for practical turbulent simulations, the lowest order gyrokinetic theory may be enough to determine the radial electric field. This controversial issue is open to further investigation.

Another important physics ingredient is to model a fusion plasma open system. While the gyrokinetic Vlasov–Maxwell system shown in section 2.2 is an isolated system, a fusion plasma is essentially an open system with sources and sinks. A straightforward approach may be to add a source term S_s to the rhs of the gyrokinetic equation (17). We then have the gyrokinetic equation for an open plasma system,

$$\frac{\partial\bar{f}_s}{\partial t} + \left\{\bar{f}_s, \bar{H}_s\right\} = C_{\rm GY}(\bar{f}_s) + S_s. \tag{41}$$

By substituting equation (41), equation (28) yields a power balance relation in the open system,

$$\sum_s \int \bar{H}_s \frac{\partial\bar{f}_s}{\partial t}\mathcal{J}_s\mathrm{d}^6\bar{Z} = \frac{\mathrm{d}}{\mathrm{d}t}\left(E_k + E_\phi + E_{A_\parallel}\right) = \frac{\mathrm{d}}{\mathrm{d}t}\left(E_C + E_S\right), \tag{42}$$

$$\frac{\mathrm{d}E_C}{\mathrm{d}t} = \sum_s \int \bar{H}_s C_{\rm GY}(\bar{f}_s)\mathcal{J}_s\mathrm{d}^6\bar{Z}, \tag{43}$$

$$\frac{\mathrm{d}E_S}{\mathrm{d}t} = \sum_s \int \bar{H}_s S_s \mathcal{J}_s\mathrm{d}^6\bar{Z}. \tag{44}$$

In the original Boltzmann equation, the system conserves the total energy in the sourceless limit $S_s \to 0$, i.e. the collisional energy transfer $\mathrm{d}E_C/\mathrm{d}t = \sum_s\int[m_s v^2/2 + e_s\phi(\boldsymbol{q})]C(f_s)\mathrm{d}^3q\,\mathrm{d}^3p$ vanishes because the collision operator locally conserves particle and kinetic energy moments. In the drift-kinetic limit $k_\perp\rho_s \to 0$, $C_{\rm GY}(\bar{f}_s) = C(\bar{f}_s)$ and thus it is easy to show that $\mathrm{d}E_C/\mathrm{d}t = \sum_s\int[m_s u^2/2 + \mu B_0 + e_s\Psi(\boldsymbol{R})]C(\bar{f}_s)\mathcal{J}_s\mathrm{d}^6Z = 0$ is satisfied. However, it is not so trivial to write a gyro-averaged collision operator including FLR effects, which keeps relevant conservation properties and a vanishing collisional energy transfer. In [52], an operator, which globally conserves particle, momentum and kinetic energy moments, was given including FLR corrections. However, the collisional power transfer does not trivially vanish because of non-local features of these conservation properties and of the gyro-averaged perturbation $\langle\Psi\rangle_{\bar{\xi}}$: we have $\mathrm{d}E_C/\mathrm{d}t = \sum_s\int[m_s\bar{u}^2/2 + \bar{\mu}B_0 + e_s\langle\Psi\rangle_{\bar{\xi}}(\bar{\boldsymbol{R}},\bar{\mu})]C_{\rm GY}(\bar{f}_s)\mathcal{J}_s\mathrm{d}^6Z = \sum_s\int e_s\langle\Psi\rangle_{\bar{\xi}}(\bar{\boldsymbol{R}},\bar{\mu})C_{\rm GY}(\bar{f}_s)\mathcal{J}_s\mathrm{d}^6Z \neq 0$. This issue is still open to further investigations.

Another traditional approach in modelling an open plasma system is to introduce a multi-scale expansion with respect to a smallness parameter $\epsilon_g = \rho_s/L_n$ [7]. In this approach, we consider a quasi-steady plasma in a source free region, and separate the gyro-centre Hamiltonian into its static and perturbed parts,

$$\bar{H}_s = \bar{H}_{0s} + \delta\bar{H}_s, \tag{45}$$

$$\bar{H}_{0s} = m_s\bar{u}^2 + \bar{\mu}B_0 + e_s\langle\phi_0\rangle_{\bar{\xi}}, \tag{46}$$

$$\delta\bar{H}_s = e_s\langle\tilde{\Psi}\rangle_{\bar{\xi}}, \tag{47}$$

where ϕ_0 is a static part of the electrostatic potential and $\tilde{\Psi} = \Psi - \phi_0$. By substituting equation (45) and $\bar{f}_s = f_{0s} + \delta\bar{f}_s$, the gyrokinetic equation (41) yields

$$\{f_{0s}, \bar{H}_{0s}\} = C_{\mathrm{GY}}(f_{0s}), \tag{48}$$

$$\frac{\partial\delta\bar{f}_s}{\partial t} + \{\delta\bar{f}_s, \bar{H}_{0s}\} + \{f_{0s}, \delta\bar{H}_s\} + \{\delta\bar{f}_s, \delta\bar{H}_s\} = C_{\mathrm{GY}}(\delta\bar{f}_s), \tag{49}$$

where the nonlinearity is retained in equation (49). In solving equation (48), the equilibrium distribution is further expanded as $f_{0s} = f_{00s} + f_{01s} + \cdots$, and from the lowest order equation, $v_\parallel \boldsymbol{b}\cdot\nabla f_{00s} = C_{\mathrm{GY}}(f_{00s})$, f_{00s} is given as a local Maxwellian distribution $f_{\mathrm{M}s}$, while f_{01s} is determined by the neoclassical theory [41, 42]. It is noted that in equation (49) $\delta\bar{f}$ is defined with respect to a collisional equilibrium distribution f_{0s}, and therefore, this approach is applicable also to non-axisymmetric configurations which do not have an exact collisionless equilibrium distribution in general. By writing equation (49) in other gyro-centre coordinates $(\bar{\boldsymbol{R}}, \bar{\varepsilon}, \bar{\mu}, \bar{\xi})$ and keeping the lowest order terms in ϵ_g, we obtain a familiar expression of the local gyrokinetic equation [7],

$$\left[\frac{\partial}{\partial t} + v_\parallel\boldsymbol{b}\cdot\nabla + \frac{c}{e_sB_0}\boldsymbol{b}\times\left(e_s\langle\tilde{\Psi}\rangle_\xi + m_sv_\parallel^2\boldsymbol{b}\cdot\nabla\boldsymbol{b} + \bar{\mu}\nabla B_0\right)\cdot\nabla\right]\bar{h}_s$$
$$= C_{\mathrm{GY}}(\delta\bar{f}_s) - \left(e_s\frac{\partial\langle\tilde{\Psi}\rangle_\xi}{\partial t}\frac{\partial f_{\mathrm{M}s}}{\partial\varepsilon} + \frac{c}{B_0}\boldsymbol{b}\times\nabla\langle\tilde{\Psi}\rangle_\xi\cdot\nabla f_{\mathrm{M}s}\right), \tag{50}$$

where $\delta\bar{f}_s = \delta\bar{H}_s\partial f_{\mathrm{M}s}/\partial\bar{\varepsilon} + \bar{h}_s$. A flux-tube simulation solves equation (50) in field-aligned coordinates with radial periodic boundary condition with phase-shift reflecting the magnetic shear [61, 62]. This model is an open system developed to study local quasi-steady turbulent transport with fixed background profiles. Although the conservation properties in the original gyrokinetic equations are lost, the quality of the nonlinear simulation is often tested using the entropy balance relation.

3. Numerical models

3.1. Numerical schemes

Solving the set of gyrokinetic equations is a rather formidable task. To summarize, we have an equation of evolution for the distribution function f in a 5D phase space, equation (17), a set of five coupled ordinary differential equations for the orbits, equations (18)–(20), and 3D integral-differential equations for the fields, Poisson's—or quasi-neutrality—equation, equation (26), and, if magnetic perturbations are also considered, Ampère's law, equation (27). This set of equations is nonlinear, with nonlinearities essentially contained in the $\boldsymbol{E}\times\boldsymbol{B}$ and $E_\parallel$ terms in the rhs of equations (18) and (19), respectively. (The nonlinearities in the polarization and magnetization are often neglected, which is probably justified in the core as long as $|\delta n|/n_0 \ll 1$, but less so in the edge.) Last but not least, the background geometry of the magnetic confinement configuration is not trivial and introduces a very strong anisotropy in the perturbations: more details on this aspect will be presented in the following subsection. Analytical methods to solve these equations are restricted to a few limiting cases and will not be discussed here. However, it should be recalled that these can serve as important verification checkpoints for numerical codes.

There are three classes of numerical methods that have been used so far to solve the set of GK equations. First, the Lagrangian approach, figure 4, consists in sampling initial positions in phase space (loading of markers), following marker orbits in 5D (pushing) and obtaining the source terms for the field equations at every timestep (charge and current assignment). The Lagrangian approach is often referred to as 'particle-in-cell' (PIC), in reference to the well-known technique described in [63]. It was introduced very early [8] in the context of gyrokinetics. Second, the Eulerian approach, figure 5, consists in discretizing the phase space on a fixed (usually structured) grid, and applying finite differences, finite volume and/or Fourier transforms for the differential and integral operators. The Eulerian approach is sometimes referred to as 'Vlasov'. Third, the semi-Lagrangian approach, figure 6, which uses a fixed phase space grid and obtains the values of f at the next timestep by tracing the orbits ending at each grid point back in time and interpolating f at the foot of the orbit. Common to all three is the need to solve for the field equation(s) in 3D configuration space: finite differences, Fourier or finite element methods have been applied.

The three classes of methods each have their own advantages and drawbacks. Several codes are based on the Lagrangian-PIC approach, e.g. GTC [64], GT3D [65], ORB5 [66], PG3EQ [67], GTS [68], as well as Parkers' [69] and Sydora's [70] (the list is not exhaustive). Lagrangian methods can be interpreted statistically [71]. The charge and current assignment can be viewed as a Monte Carlo integration having an error proportional to $\sqrt{\mathcal{V}/N}$ where N is the sample size, i.e. the number of markers, and $\mathcal{V}$ is the variance of the estimator. The main difficulty with such methods is the accumulation of these sampling noise errors in the course of a simulation [72], which can lead to either an overestimate [66] or an underestimate [73] of the transport level, making this issue particularly delicate. Diagnostics of signal/noise ratio [73], as well as other physics based quantities such as the entropy balance [74–76] and the energy conservation property [66, 77, 78] are extremely useful tools to estimate the quality of a simulation. (Empirically, it has been found that a signal/noise ratio above 10 is necessary in order to have credible simulation results. Typically, this requires of the order of 100–200 markers per cell used for the numerical representation of the fields. If a Fourier filter is applied then it is the number of markers per Fourier mode retained in the filter that matters.)

Reducing the error can be achieved by increasing the number of markers N or decreasing the variance $\mathcal{V}$ of the

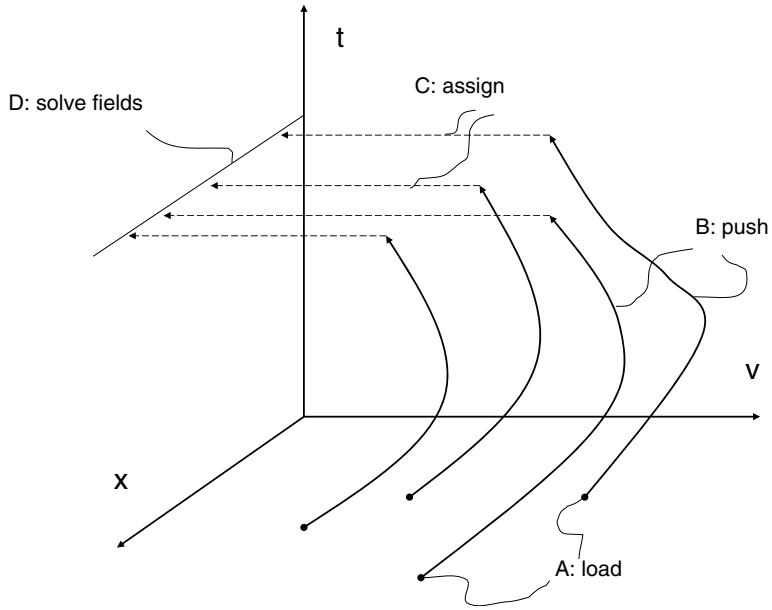

Figure 4. In Lagrangian-PIC methods, marker initial positions are loaded pseudo- (or quasi-) randomly in phase space (A). Markers are evolved along their orbits (B). Charge and current perturbations are assigned (projected) to real space (C). Field equations are solved (D), e.g. on a fixed grid in real space.

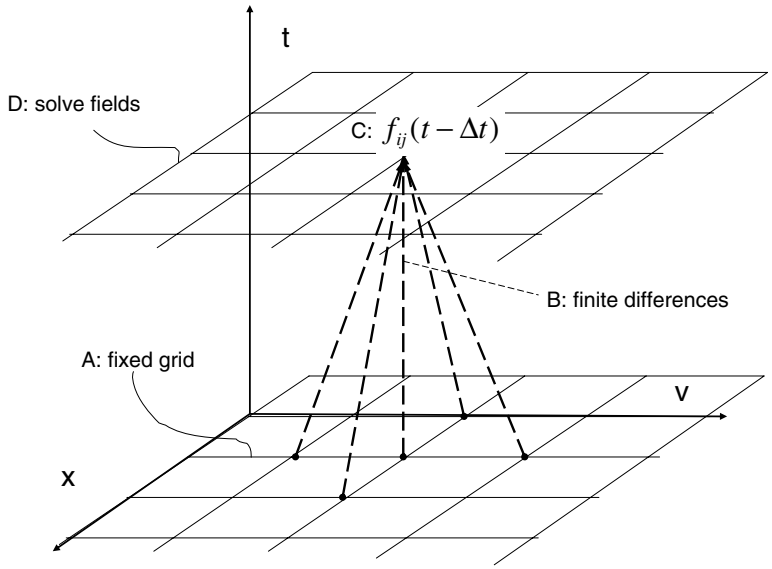

Figure 5. In Eulerian methods, a fixed grid is defined in phase space (A). Finite difference expressions are used (B) in order to obtain the value of f at grid points at the next time step (C). Field equations are then solved (D) after integration over velocity space.

estimator. Indefinitely increasing N is not possible due to the cpu time limitation: nonlinear gyrokinetic simulations are very demanding in computer resources. Thus, several *control variates* methods to reduce $\mathcal{V}$ have been applied. First, instead of discretizing the whole distribution function f using markers, it is better to write $f = f_0 + \delta f$, with f_0 a given function of phase space coordinates, and use markers to discretize δf only. The f_0 contribution to the charge or current is treated analytically and is usually considered as an equilibrium distribution function $f_0 = f_{\rm eq}$. The question of the choice of $f_{\rm eq}$ will be discussed in the next subsection. To obtain δf, an equation of evolution is integrated numerically along the perturbed orbits: this is called the 'δf scheme' [69, 79–81]. More precisely, δf is written as a weighted Klimontovitch distribution, with the particle weights $w_{\rm p} = \delta f/g$, g being the PDF of the distribution of markers in phase space. The quantity $1/g$ can be viewed as the phase space volume 'represented' by the marker and is conserved along the marker motion (Liouville theorem). Another approach is to obtain δf directly from the constancy of f along orbits $Z(t)$: $\delta f = f(Z(t)) - f_0(Z(t))$ [82]. For core turbulence, we have $|\delta f| \ll f_{\rm eq}$, and the sampling error is thus reduced by the corresponding large factor. Further improvements to the δf scheme have been devised, in particular in order to treat electromagnetic (EM) perturbations, such as split-weight schemes [83–85]. The idea is to separate out the adiabatic response, $f = f_0 + f_0 e\phi/T + \tilde{\delta f}$,

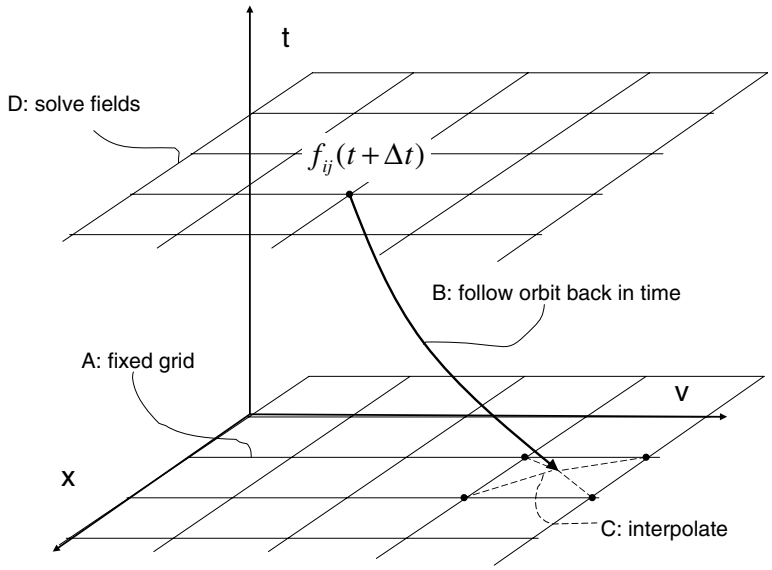

Figure 6. In semi-Lagrangian methods, a fixed grid is defined in phase space (A). The orbits are integrated back in time from each grid point (B). The value of f at grid points is obtained by interpolation at the foot of the orbit (C) and using the property $f = \text{const}$ along orbits. Field equations are then solved (D) after integration over velocity space.

for electrostatic perturbations, which has been generalized to $f = f_0 + f_0 e\delta\psi_{\text{eff}}/T + \tilde{\delta f}$, with $\delta\psi_{\text{eff}} = \delta\phi + \int \partial A_\parallel/\partial t \, \mathrm{d}x_\parallel$ for electromagnetic perturbations. A difficulty with EM perturbations lies in the existence of two large terms in Ampère's equation that should cancel out: this is known as the *inaccuracy* or the *cancellation* problem, which is particularly severe for long wavelength modes and $\beta_e > m_e/m_i$. A generalization of the split-weight scheme was shown in [85] to overcome the problem. Another option is to use an enhanced, adjustable control variates technique [86], in which the key idea is to replace as much as possible of the Monte Carlo integration for charge and current assignment with analytic calculations. It was shown that the required number of markers could thus be reduced by orders of magnitude for EM modes in the long wavelength limit. For EM simulations, fluid-kinetic hybrid electron models have been proposed, e.g. in [87], which have the specific feature of removing the tearing mode analytically, thus being less demanding for the numerical resolution and improving the numerical properties.

Note, however, that Alfvén waves have been successfully simulated with the Lagrangian-PIC approach and all plasma species treated kinetically [88], i.e. without using the fluid-hybrid model.

Another way to reduce marker noise is *importance sampling* [71, 77], a famous example of which is the Metropolis algorithm [89] introduced more than 50 years ago for Monte Carlo computations of equations of state. In our context, this consists in choosing adequately the marker distribution g so that it is large in regions of phase space which have large perturbations. The simple way to prescribe $g \propto f_{\text{eq}}$, known as proportional loading, is far from being adequate: it is shown in [78] that a substantial gain in the quality of the simulation can be obtained by applying an optimized loading scheme.

Generally speaking, controlling noise is necessary in order to preserve important physical properties such as zonal flow structures. The relevant quantity is the number of markers per numerical degree of freedom of the field representation. Thus, various filtering techniques have been applied in Lagrange-PIC simulations; a striking example is a magnetic field-aligned Fourier filter [66] that takes advantage of the strong anisotropy of the perturbations.

Eulerian schemes are not subject to the issue of maker sampling noise which is critical in Lagrangian-PIC methods. On the other hand, when explicit time integration is applied, they are subject to the Courant–Friedrichs–Lewy (CFL) stability condition [90, 91], which constrains the maximum time step as a function of grid space resolution. Several gyrokinetic codes use this approach, such as GS2 [92, 93], GYRO [94], GENE [95, 96], GKV [97], GKW [98] and GT5D [58, 99]. Note that a way to circumvent the CFL restriction is to use implicit or semi-implicit time integration schemes [99]. The success of Eulerian schemes relies in particular on an accurate and stable treatment of the $\boldsymbol{E} \times \boldsymbol{B}$ nonlinearity. In flux-tube codes such as GS2 and GKV this is successfully resolved using spectral Fourier methods and anti-aliasing procedures. Such methods are applicable if the system has background symmetry and periodic boundaries. However, global approaches cannot use this approach and this is why different Eulerian (and semi-Lagrangian) schemes have been explored. Another issue is that finite difference schemes introduce numerical dissipation, which has to be assessed by grid convergence studies. Fortunately, this numerical dissipation is also what makes steady-state simulations possible as will be discussed in section 3.3. On the other hand, while one would like to keep numerical dissipation as small as possible (in the sense that it should have a benign effect on the physics of interest), there is, generally speaking, a trade-off between this dissipation and the overshoot problem: high order finite difference schemes can result in unphysical oscillations. In particular, the positivity of f is not guaranteed, unless special algorithms are devised to this effect, such as the positive flux conserving method [100]. Conservative finite difference schemes [101] have also been

introduced [58, 99] and their impact in helping to obtain long, steady-state simulations is exposed in section 3.3.

Given the respective difficulties faced by Lagrangian-PIC and Eulerian simulations, a third approach, called semi-Lagrangian, has been pursued [102–104]. The idea is to benefit from the best of two worlds, i.e. on the one hand using characteristics so as to remove the CFL restriction inherent in explicit Eulerian methods and, on the other hand, using a regular Eulerian grid so as to avoid the statistical noise problem inherent in Lagrange-PIC methods. The technique of operator splitting is applied in order to avoid multi-dimensional interpolations. The main difficulty lies in finding an appropriate interpolation scheme, where a trade-off between dissipation and overshoot has to be found. High order interpolation schemes are less dissipative but can lead to unphysical oscillations and negative f regions [105]. In order to address this problem the ENO/WENO (weighted/essentially non-oscillatory) schemes have been developed, which are generalizable to arbitrary high order interpolation in smooth regions while avoiding spurious oscillations in non-smooth regions [106, 107]. Another delicate point to consider is the issue of particle conservation which, even if only small errors are made, can lead to large errors in the potential. Conservative semi-Lagrangian schemes have, to our knowledge, not yet been developed.

The implementation of collision operators is more straightforward in Eulerian and semi-Lagrangian than in Lagrangian-PIC or δf formulations, because the partial derivatives in velocity space that these operators involve are readily available from the phase space grid discretization. Several Eulerian gyrokinetic codes include collision operators [52, 92, 94, 96, 97] the technical difficulty residing in the timestep limitation due to stability criterion in explicit schemes, which can be circumvented by partly implicit schemes.

In Lagrangian PIC, the information about velocity dependence of the distribution function has to be reconstituted through a binning process, which can be both time consuming and subject to statistical sampling errors. The approach usually followed is a Langevin–Monte Carlo formulation: collisions, acting as a diffusion in velocity space, are modelled as a random walk process [51, 108]. The markers, on top of their deterministic evolution, equations (18)–(20), are given randomly chosen kicks at every time step. The distribution of these kicks is chosen so as to describe, in a statistical averaged sense, the time evolution of f due to collisions. This has been applied to several situations, including electron–ion collisions [37], neoclassical simulations [54, 109–111] and ion–ion collisional damping of zonal flows [112]. The main drawback of this technique is that it leads to an increase in statistical noise, described in terms of 'weight spreading', for which a solution is proposed in [113]. Indeed, the weights must now be interpreted as a random variable field with a finite variance as an additional dimension of phase space [114]. A low-noise collision operator scheme for PIC simulations is introduced in [115] that does not invoke the Langevin–Monte Carlo approach.

Gyrokinetic turbulence simulations are extremely demanding in computer resources and require to be run on the most performing platforms. These are massively parallel, involving thousands of processors. Thus, in order to take advantage of the evolution of HPC (high performance computing), turbulence gyrokinetic codes must be parallelized [64, 116]. Several strategies can be pursued to this effect, for example domain decomposition, in which different processors solve for a different portion of the whole phase space domain. Domain decomposition is in principle applicable to all three classes of schemes (Lagrangian, Eulerian and semi-Lagrangian). In addition, a domain cloning technique can be applied, which is useful in particular for Lagrangain-PIC codes, in which all processors of a clone family contain identical real space information (i.e. field quantities) but different markers [117, 118]. In all these algorithms, communications between processors are involved, and it is crucial that these communications do not dominate the computing time. The question of scalability is important, i.e. on how the performance of the code improves when increasing the number of processors. The scalability is measured in strong scaling tests (a problem of fixed size is given to an increasing number of processors) and weak scaling tests (problems whose size increases with the number of processors). It must be noted that the most demanding inter-processor communication type is the one in which all processors have to exchange information with all others ('all-to-all'). This occurs typically when data have to be transposed, e.g. when Fourier transforms are computed in the direction of the domain decomposition, and strategies have been developed to nevertheless allow for a good parallel efficiency.

3.2. Geometry, locality, globality

A prominent feature of turbulence in magnetic fusion plasmas, which distinguishes it from turbulence in neutral fluids, is the importance of geometrical aspects brought about by the presence of the background magnetic field. This introduces a strong anisotropy of the low frequency perturbations. As a result of the gyrokinetic ordering, these have very long wavelengths in the parallel direction, $k_\parallel \rho_s \sim \rho_* \ll 1$, whereas the perpendicular wavelength spectrum extends down to the Larmor radius scale. Moreover, core plasmas are very weakly collisional, with a mean free path larger than the system size. Consequently, the geometry of the magnetic configuration strongly affects microinstabilities and turbulence.

The anisotropy can be used to the advantage of numerical schemes: the use of field-aligned coordinates brings an order of magnitude improvement in all approaches (Lagrangian, Eulerian and semi-Lagrangian) described in the previous section. A further simplification is made in *flux-tube* codes, in which the domain considered is a vicinity of a magnetic field line. The equations are expanded in this vicinity such that all coefficients are constant: for kinetic profiles, $f_0 = \text{const}$, $\partial f_0/\partial x = \text{const} \Rightarrow T = \text{const}$, $\mathrm{d}T/\mathrm{d}x = \text{const}$, $\mathrm{d}n_0/\mathrm{d}x = \text{const}$ and for geometrical coefficients, all metric tensor elements are assumed to be constant $\Rightarrow q = \text{const}$, $\hat{s} = \text{const}$. Typically, periodic boundary conditions are prescribed, which is justifiable for the coordinates within a magnetic surface, but less so in the radial direction. More precisely, periodic radial boundary conditions are correct in the limit of infinite system size ($\rho_* \to 0$) and infinite computational box radial size. From a practical point of view, the radial extent of the computational box should be chosen much larger than the

radial turbulence correlation length. This can be challenging in particular for ETG simulations in which very elongated perturbations (streamers) are generated. Profile variations and large scale relaxations are not described in flux-tube codes. In other words, the radially averaged gradients are frozen in such simulations. Moreover, the shearing of equilibrium profiles is absent. Equilibrium density and temperature gradient profile shearing was shown to have an important incidence when studying finite size effects (ρ_* scaling) [119]. Global codes, on the other hand, take the geometry of the whole plasma domain into account. Unlike flux-tube codes they do not make use of radial periodic boundary conditions. In truly global models, the profiles are left to evolve without *a priori* constraint, and thus can describe phenomena such as profile shearing, profile relaxation and avalanche propagation [120] in a consistent manner. Flux-tube codes are still very useful. In particular, they can serve as a valuable cross-check of global codes, the results of which have been shown to agree for sufficiently small ρ_* [119].

Another issue is related to the treatment of the regions near to the boundaries of the computational domain. Some codes use 'buffer zones' at both inner and outer sides of the radial domain so as to dampen the perturbations of the distribution function and of the fields. This results in simulations with fixed average radial gradients. Other codes do not make use of buffer zones and let the distribution function and the fields evolve freely with, on magnetic axis, only a regularity condition (unicity condition) [66]. While there is, physically speaking, no true boundary on the inner side, the question of the outer boundary is more delicate. Most gyrokinetic codes focused on core turbulence circumvent this problem by assuming a region of small enough (sub-critical) gradients in the vicinity of the 'edge', so that turbulent perturbations die out before reaching the boundary of the computational domain. Coupling of core gyrokinetic turbulence codes with edge turbulence codes is still largely an open field of research. Not only is the physics in the SOL different but also the topology of magnetic field lines changes from closed to open with, in addition, the complication due to the presence of the magnetic separatrix in diverted discharges.

The geometrical complexity of the magnetic configuration is taken into account to various degrees in the different gyrokinetic codes. Essential geometrical features include the magnetic curvature, safety factor and shear. Simplified equilibrium models, e.g. the so-called s–α model, which assumes circular shifted magnetic surfaces, have been used in gyrokinetic computations, including the well-known Cyclone benchmark [121]. Other models consider more shaping effects and rely on a local equilibrium model [122] that takes into account finite aspect ratio, elongation and triangularity. Some codes use ideal MHD axisymmetric toroidal equilibria without further approximation directly obtained from Grad–Shafranov solvers [123]. Most of the existing codes assume an axisymmetric toroidal configuration applicable to tokamaks. There has recently also been an effort for gyrokinetic simulations in 3D stellarator configurations both for flux-tube [124–126] and for global [127, 128] codes.

Geometrical aspects also affect the equilibrium distribution function $f_{\rm eq}$. In global collisionless gyrokinetics, $f_{\rm eq}$ is a function of the unperturbed constants of motion. In axisymmetric systems, these are ε, μ and the canonical angular momentum p_φ. The latter is proportional to $\psi_0 = \psi + (q/m)(I/B)v_\parallel$, where ψ is the equilibrium magnetic poloidal flux and $I = I(\psi) = RB_{0\varphi}$. In some formulations of the δf scheme ($f = f_0 + \delta f$) the choice $f_0 = f_{\rm eq}$ is assumed but the local approximation $\psi_0 \approx \psi$ is made for the functional dependence of $f_{\rm eq}$ and the time variation of f_0 along unperturbed orbits is neglected. The error made in neglecting the variation of f_0 along unperturbed orbits is proportional to the equilibrium variation over an orbit width, and thus is more pronounced in small systems (large ρ_*) and regions of large gradients (e.g. transport barriers). Most importantly, this choice is not consistent and can lead to the spurious growth of zonal $\boldsymbol{E} \times \boldsymbol{B}$ flows in the early stages of the simulation [129] or to spurious oscillations in the late nonlinear phase [65]. Similar problems are found in full-f algorithms when the simulations are initialized with $f_{\rm init} = f_0$ a function of ψ instead of $f_{\rm init} = f_{\rm eq}$ a function of ψ_0 [130]. The solution is to choose a canonical initial distribution function [65, 129, 130]. Note that if the flux-tube approach is adopted or if another similar local approximation is made, the radial variation of $f_{\rm eq}$ is neglected (while its radial gradient is kept, which means there is an inconsistency between $f_{\rm eq}$ and its gradient) and therefore the variation of $f_{\rm eq}$ along unperturbed orbits is anyway neglected (which is correct only in the $1/\rho_* \to \infty$ limit). This should be kept in mind when comparing flux-tube and global codes. Finally, we recall that a physically relevant equilibrium distribution function in the presence of gradients naturally involves radial electric fields and implies the inclusion of collisional effects as discussed in section 2.3. Moreover, for non-axisymmetric (or non-helically symmetric) configurations there exists no collisionless $f_{\rm eq}$ with radial gradients, because of the lack of conservation of p_φ, and a consistent description with collisions and electric fields is a conceptual necessity. Other differences exist in the geometrical treatment, such as for the flux-surface-averaged potential $\langle\phi\rangle_{\rm f}$ (which appears in the expression of the electron Boltzmann term in the quasi-neutrality equation when adiabatic electrons are assumed). For example, the poloidal dependence of equilibrium coefficients appearing in the quasi-neutrality equation is sometimes neglected so as to obtain a decoupled equation for $\langle\phi\rangle_{\rm f}$. Neglecting this toroidal linear coupling for the zonal flow term can result in a change on its dynamics [3]. It should be noted that the correct expression for $\langle\phi\rangle_{\rm f}$ implies that the quasi-neutrality equation is a differential–integral form. In axisymmetric systems this means a non-local operator in the poloidal coordinate. In 3D configurations, the non-locality is for both poloidal and toroidal coordinates, which poses technical difficulties due to the large computer memory requirement for the field solver.

3.3. Conservation properties and statistical convergence

The system of gyrokinetic equations satisfies a number of conservation properties such as particle, momentum and energy. In addition, the evolution of entropy should satisfy a balance equation. Simulations based on this theory should verify these properties as a part of the determination of their numerical accuracy. Turbulent processes responsible for transport are chaotic in nature, and thus the predictions made by direct numerical simulations have a statistical aspect. The aim

is thus to obtain long enough, statistically converged, 'steady-state' simulations.

The issue of energy conservation is intimately related to the formulation of the gyrokinetic equations and to the presence of the parallel velocity nonlinearity (PVN), resulting from the first term on the right-hand side of equation (19) and the perturbed part of the distribution function. More precisely, writing formally $\bar{f}_s = \bar{f}_{0s} + \delta\bar{f}_s$, with $\bar{f}_{0s}$ a time-independent (equilibrium) distribution function, the PVN is a contribution to equation (17) which can be written as

$$-\frac{\boldsymbol{B}^*}{m_s B_\parallel^*}\cdot e_s \nabla\langle\Psi\rangle_{\bar{\xi}} \frac{\partial \delta\bar{f}_s}{\partial \bar{u}}. \tag{51}$$

From the gyrokinetic ordering point of view, it can be shown that this term is an order smaller than the $\boldsymbol{E}\times\boldsymbol{B}$ *nonlinearity*, resulting from the third term of the right-hand side of equation (18) and the perturbed part of the distribution function, in other words a contribution to equation (17) which can be written as

$$\frac{c}{e_s B_\parallel^*}\boldsymbol{b}\times e_s\nabla\langle\Psi\rangle_\xi \cdot \frac{\partial \delta\bar{f}_s}{\partial \bar{\boldsymbol{R}}}. \tag{52}$$

On the basis of this argument, the PVN has been neglected in several gyrokinetic codes.

After careful checking of the numerical convergence properties, using both Eulerian and Lagrangian-PIC codes in both straight and toroidal geometries, the smallness of the physical effect of the PVN on ITG turbulence and zonal flow dynamics has been confirmed [75, 131, 132]. However, verifying the energy conservation property (which is violated if the PVN is neglected) is a very useful check of the accuracy of the numerical simulation [77]. Moreover, retaining the conservative nature of the original gyrokinetic equations and reflecting this nature as faithfully as possible in the numerical formulation has been shown to be beneficial: a non-dissipative conservative finite difference scheme [101] has been used in the Eulerian code GT5D [75, 99] resulting in a stabilizing influence, especially for long-time simulations.

In [38, 133] it was shown that some dissipation must be present in the system in order to get a statistical steady state for all quantities in the simulation. Whereas in Eulerian methods numerical dissipation of the distribution function is present due to the discretization, this is not the case for Lagrange-PIC methods for which the filamentation of phase space (see below) can lead to a statistical sampling noise problem (rather than dissipation). Consequently, for collisionless cases the fluctuation entropy indefinitely increases in time, even though lower order moments of f like the energy flux may seem to have reached steady state [74]. This has been known as the *entropy paradox*. A generalized thermostat (W-stat) was proposed in [133] as a way to resolve the problem. In PIC methods the entropy increase is also accompanied by an indefinite increase in particle noise, due to the fact that the mean-square marker weights, $\langle w_p^2\rangle$, grow secularly: this quantity is approximately proportional to both the sampling noise and to the numerical entropy. In [134], a noise-control algorithm based on a W-stat has been successfully applied using modified Krook operators, allowing for long, steady-state simulations. In [76] the entropy balance relation is verified using this noise control operator and it is shown for the first time that statistical steady-state turbulence simulations can be reached with the Lagrangian-PIC approach, thus ending a longstanding controversy. Another technique successfully applied is coarse graining, which consists in periodically smoothing the particle weights in small regions of phase space [135].

For Eulerian codes the issue of statistical steady state is also important. Collisionless gyrokinetics leads to an indefinitely thin *filamentation* of phase space [97] that is sooner or later missed by the finite size grid. In Eulerian schemes there is usually, in addition to physical dissipation, a finite numerical dissipation related to the finite difference algorithms used. This numerical dissipation can in fact help the simulation to reach steady state. For example, using the GYRO code [94], it is shown in [136] that the entropy production by filamentation is balanced by entropy dissipation by the upwind scheme, thus simulations can reach a statistically converged steady state. Sometimes a numerical hyperdiffusion term has to be added to the equations in order to stabilize the scheme. Weak collisions also lead to a statistical steady-state, which can be understood as a result of entropy generation, transfer and dissipation at small scales in phase space [40, 97]. Another approach, based on physical dissipation with pitch angle and energy scattering effects, has been pursued in the GKV [97], GYSELA [55], TEMPEST [56] and GT5D [58] codes.

The extent to which simulation results such as the turbulent transport fluxes depend on the used dissipation mechanism is still an open question. Detailed comparisons, e.g. of the zonal flow saturation level, should be made between the different models.

3.4. Benchmarking

Given the fact that gyrokinetic nonlinear turbulence simulations are extremely demanding in computing resources, these simulations are often run at the limit of the available power and, consequently, the various limitations of each numerical scheme are often put to the test. Moreover, as should be clear from the above subsections, there are substantial differences in the actual implementation of the gyrokinetic equations in the various codes, relative e.g. to the geometrical model used, the type of nonlinearity retained, the electrostatic or electromagnetic nature of perturbations, the way sources are implemented, the locality (flux tube) or globality, etc. Thus it is very important that the various approaches and codes be compared with each other in their common domain of validity. This is part of a more general validation and verification exercise for which best practices are exposed in [137].

For ITG instability and turbulence in tokamak plasmas, an important benchmarking exercise was undertaken in [121], for which a set of parameters, known as the 'cyclone' base case, was defined inspired from DIII-D H-mode experiments [138]. Interestingly, these were aiming at investigating the effects of plasma shaping, in particular elongation, on the confinement performance. However, the cyclone base case was run using a simplified geometrical model of circular concentric magnetic surfaces cross-section and local flux-tube codes, with the notable exception of the global code from Sydora [70].

Linear tests imply a comparison of the spectra of real frequencies and growth rates of the most unstable modes,

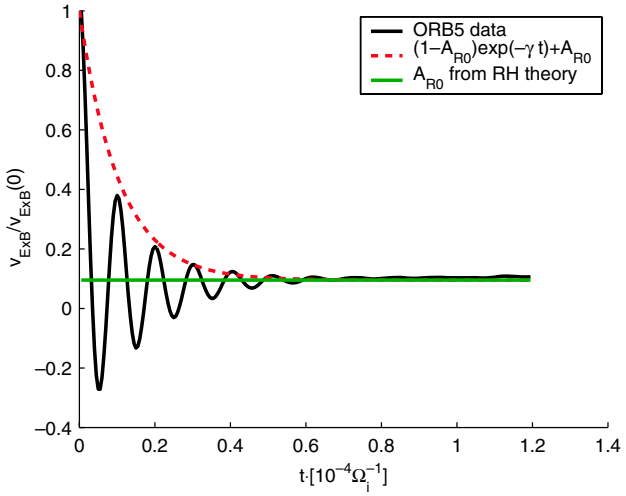

Figure 7. Zonal flow and geodesic acoustic mode (GAM) damping test, showing the time evolution of the $\boldsymbol{E} \times \boldsymbol{B}$ velocity from an initial perturbation. The continuous black line is the global gyrokinetic simulation result obtained with the ORB5 code [66], the dashed line is the analytical estimate of amplitude taking into account GAM damping [204, 205] and the horizontal line is the undamped residual as predicted in [139].

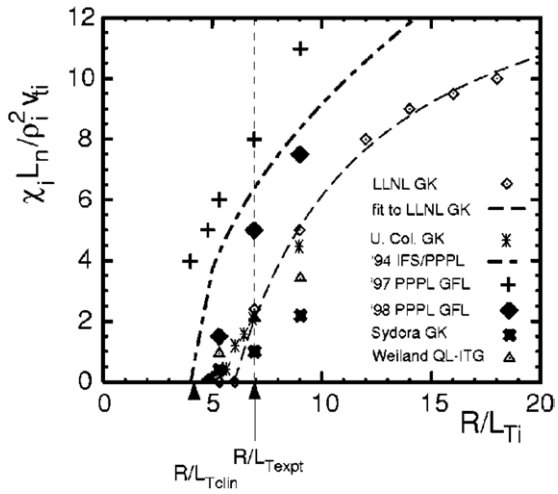

Figure 8. Normalized ion heat diffusivity as predicted by gyrofluid codes using different closures (crosses and filled diamonds), flux-tube gyrokinetic codes (open diamonds and stars), a global gyrokinetic code (X) and a quasi-linear multi-mode model (triangles). All models assume adiabatic electrons. For more details see [121].

for which good agreement was reported between global and flux-tube gyrokinetic and gyrofluid codes (see figure 1 of [121]). This agreement extends also to the predicted value of the critical gradient, $(R/L_T)_{\rm crit} \approx 4.0$. Another important linear test is on the undamped residual zonal flow (ZF) level resulting from an initial perturbation, as predicted analytically by Rosenbluth and Hinton [139] (see figure 2 of [121]). This test was essential in explaining the origin of the discrepancy between gyrokinetic and gyrofluid models, which overestimated the ZF damping and thus predicted a higher estimate of ITG transport. However, it is still unclear whether a correct treatment of the undamped residual zonal flow is enough to remove all discrepancies: there is, generally speaking, a more complex interaction of turbulence with zonal flows, e.g. 'geodesic transfer' [140]. Therefore nowadays tests also include the transient excitation of geodesic acoustic modes (GAMs) and a measure of their frequency and damping rate. An example with the ORB5 code [66] is shown in figure 7. Thus, a verification of the proper treatment of axisymmetric modes can be made.

Nonlinear cyclone predictions of heat diffusivity (see figure 8, from [121]) have shown important differences between gyrofluid and gyrokinetic codes. Due to the incomplete physics related to the treatment of the zonal flows in gyrofluid models, the predicted level of transport was overestimated (various modifications of the radial drift closure and FLR terms [141, 142] can help to improve the comparison between gyrofluid and gyrokinetic simulations). Gyrokinetic models predict a vanishingly small transport just above the linear critical gradient, interpreted as turbulence suppression by zonal flows, and resulting in an upshifted value of the temperature gradient above which transport takes off (the so-called 'Dimits shift'), $(R/L_T)_{\rm eff} \approx 6.0$. The fast increase in transport above this upshifted effective critical gradient implies *profile stiffness*: as a consequence, a large increase in input power results in only a small increase in temperature gradient.

Incidentally, this stiffness makes true predictions and comparisons (between codes and with experiments) difficult for gradient-driven simulations, and can result in substantial differences. For example, for the cyclone base case parameters, the predicted transport level by gyrofluid codes is a factor at least 2 higher than gyrokinetic codes [121].

Geometrical aspects are also crucial. Already for the cyclone benchmark [121] differences were noted between the simple circular concentric approximation (s–α model) and a realistic MHD equilibrium, even in linear calculations. These aspects were recently revisited [143] and the conclusion is that the main part of the discrepancy stems from inconsistencies of first order in inverse aspect ratio ε in the s–α model (even at low β), whereas very little is due to physical finite aspect ratio effects (e.g. low β Shafranov shift). The importance of having a sound basis for studying further geometrical effects (elongation, triangularity, etc) cannot be underestimated. But this is true also for finite size effects (ρ_* scaling). This has led to some controversy in the community because of apparently conflicting results as to the local limit of global simulations [119, 144], while it was shown in [143] that the discrepancy originates essentially from the s–α inconsistencies mentioned above.

Toroidal ITG benchmarking has been extended to other codes [145]: the δf Lagrangian-PIC code ORB5 [66], the full-f Lagrangian-PIC code ELMFIRE [57] and the semi-Lagrangian code GYSELA [104], all global, and the Eulerian flux-tube codes GENE [95, 96] and GKW [98, 146]. The comparisons also involve the time evolution of turbulence spectra and reasonably good agreement has been achieved.

There have been so far many fewer benchmarks of the trapped electron mode (TEM) and ITG modes with non-adiabatic trapped electron response. This is probably the most difficult electrostatic case, from the numerical point of view, because both ion and electron dynamics have to be solved simultaneously. A linear comparison of GTC [64], GT3D [65] and FULL [147] codes can be found in [148], which includes

interesting ITG to TEM transitions at short wavelengths and at small η_i values.

Simulations of ETG turbulence in tokamaks have led to some controversy, with a prediction, made with Eulerian flux-tube codes, of a high transport level [93, 95] which was attributed to the predominance of radially elongated streamers that persist in the nonlinear stage, whereas simulations made with a global Lagrangian-PIC code resulted in much lower levels of transport [149]. This has prompted a check of the impact of noise in Lagrangian-PIC simulations [72]. An ETG benchmark point was defined [150] and the origin of the discrepancy found [151] after numerical convergence studies [152] using a flux-tube Lagrangian-PIC code [67]. A further confirmation of the high level transport result was made with the global ORB5 code in a series of low-noise Lagrange-PIC simulations [73].

There has been so far no systematic code benchmarking and cross-comparison similar to the 'cyclone' case for other types of confinement than tokamaks. Nevertheless, progress has been made recently in gyrokinetic simulations of non-axisymmetric systems [124–128]. We note that defining a 'cyclone' case for 3D systems is a difficult task given the enormous parameter space characterizing the geometry of such configurations.

As a summary of this section, we conclude that having several completely different methods for the numerical resolution of gyrokinetic equations is not a luxury, but a necessity. We consider that each major code development has objectively contributed to the progression of research in the field of gyrokinetic turbulence of magnetically confined plasmas. Cross-comparisons have permitted to resolve important physical and numerical issues, and it is hoped that such comparisons will continue in the future. As the few examples mentioned above show, it is crucial that these comparisons consider the differences, sometimes only apparently benign, between the details of the implementation of gyrokinetic equations into the codes.

4. Fundamentals in gyrokinetic turbulence and transport

Fundamental ingredients of plasma turbulent transport and important concepts associated with the gyrokinetic simulations of the microturbulence in magnetic fusion plasmas are described in this section, that is, microinstabilities, zonal flows, geodesic acoustic modes (GAMs), transport scaling, etc. More detailed explanations for turbulent transport will be given in the next section.

4.1. Microinstabilities

Magnetically confined fusion plasmas with high ion and electron temperatures are filled with a variety of fluctuations observed in a wide range of spatial and temporal scales. Plasma turbulence causing the anomalous transport of particles, momentum and energy is considered to be driven by microinstabilities whose scale lengths related to ion or electron gyroradii are much shorter than equilibrium scales. Drift waves [33, 34] are destabilized by density and temperature gradients above thresholds, even if the plasma equilibrium configuration is stable to the magnetohydrodynamic (MHD) instabilities. Since the first gyrokinetic simulations of drift waves in the early 1980s [8], the application area has been widely expanded as described below.

4.1.1. Ion temperature gradient mode. The ion temperature gradient (ITG) mode is believed to be responsible for the anomalous ion heat transport in magnetized plasmas with low β, where $\beta = p/(B^2/8\pi)$ for the plasma pressure p and the magnetic field strength B. No particle flux nor electron heat transport is, however, caused by the ITG turbulence with adiabatic electron response. Spatial scales of the ITG turbulence perpendicular to the confinement field is characterized by $k_\perp \rho_a \sim 0.1$–1 where the ion acoustic gyroradius $\rho_a \equiv C_a/\Omega_i$ and the ion acoustic speed $C_a = \sqrt{T_e/m_i}$. Here, m_s and T_s represent the mass and temperature of the sth species. The perpendicular phase velocity is related to the ion diamagnetic drift motion. The gyrokinetic simulations of ITG driven turbulence were first applied to a simple slab geometry [37, 153].

The toroidal ITG mode is destabilized by coupling of toroidal magnetic drift and $\boldsymbol{E} \times \boldsymbol{B}$ convection, and its linear eigenfunction has the typical ballooning structure, where the parallel scale length is characterized by the connection length qR. Here, q and R mean the safety factor and the major radius, respectively. Because of the strong anisotropy in the mode structure, the microturbulence generally exhibits a two-dimensional nature. The first gyrokinetic simulation of ITG turbulence in a global tokamak configuration was carried out in the early 1990s [154]. Theoretical and numerical models of ITG turbulence simulations were established in the early days. Specifically, the importance of turbulent-generated sheared $\boldsymbol{E} \times \boldsymbol{B}$ flows (zonal flows) and a proper treatment of the adiabatic electron response have been widely recognized through local flux-tube simulations using gyrofluid and gyrokinetic models [67, 155–158] (see also section 4.2.1 for more detailed discussions). Then, intensive simulation studies have confirmed the saturation mechanism of the toroidal ITG instability due to the turbulent-generated zonal flows which lead to a reduction in the ion heat transport and the resultant up shift of the critical temperature gradient (that is, the so-called Dimits shift) [121]. Reasonable agreement of various gyrokinetic simulations in ion heat transport flux has also been confirmed for a limited parameter space [121], which will be described in detail in section 5.1.1.

4.1.2. Trapped electron mode. If a kinetic electron response is included, the trapped electron modes (TEM) can be destabilized in a wavenumber range overlapping that of the ITG mode. The collisionless TEM mode has lower stability thresholds than those for the toroidal ITG instability, but its growth rate is decreased by increasing the collision frequency due to de-trapping of particles [45]. As a potential candidate for causing the anomalous particle and electron heat transport, the TEM turbulence is also actively investigated by means of gyrokinetic simulations [159–164], the present status of which will be described in section 5.1.2.

4.1.3. Electron temperature gradient mode. The electron temperature gradient (ETG) mode is the counterpart of the ITG mode. When the adiabatic ion/electron response is assumed and the Laplacian term is neglected in the gyrokinetic Poisson equation, the linear ETG mode is completely isomorphic to the ITG mode, while there is a difference in the adiabatic response to the zonal flow potential (see section 4.2.1). It means that the normalized gyrokinetic equation in a local flux-tube configuration has exactly the same form for the two modes except for the sign of the electric charge, where the wavenumbers and frequencies are scaled with the electron and ion gyroradii and their parallel transit time. The local ITG and ETG turbulence cause the heat transport normalized in the gyro-Bohm unit, $\rho_{ts}^2 v_{ts}/L$, where v_{ts}, ρ_{ts}, and L denote the thermal speed ($=\sqrt{T_s/m_s}$) and the thermal gyroradius ($=v_{ts}/\Omega_s$) of the sth species and an equilibrium scale length, respectively. According to the gyro-Bohm scaling, for $T_e = T_i$, the electron heat transport caused by ETG turbulence is expected to be smaller by a factor of $\sqrt{m_e/m_i}$ in real units than the ion heat transport driven by the ITG mode. This is, however, in contradiction to many observations of the strong anomaly in the electron heat transport. To explain this point, gyrokinetic simulations of the toroidal ETG turbulence have been carried out (see, e.g., [95, 165]), and their current achievements and remaining issues will be reviewed in section 5.1.2.

4.1.4. Miscellaneous. The ITG and TEM modes are stabilized as the plasma β increases. Instead, electromagnetic modes, such as the kinetic ballooning mode (KBM) or the Alfvén ITG mode [147, 166, 167], are destabilized. A transition threshold from the ITG-TEM to KBM is, typically, local $\beta \sim 1\%$ (see, e.g., [147]). Gyrokinetic simulations including the electromagnetic and kinetic electron effects have been applied to the linear KBM [78, 88, 168] as well as the KBM turbulence [169] that may be important for the anomalous transport in the high β regime.

In addition to the drift wave turbulence described above, gyrokinetic simulations are employed for other subjects such as the internal kink mode [170], the collisionless tearing mode [171], the shear Alfvén waves [88, 172] and the energetic particle transport due to microturbulence [173–175]. Application of gyrokinetics to a short-wavelength regime of the MHD turbulence in space and astrophysical plasmas is also considered in [176–178].

Several different types of microinstabilities have been briefly described above. While spatio-temporal scales of the ITG and ETG modes are different by a factor of ρ_i/ρ_e, there are overlaps in frequency and wavenumber spectra through those of the TEM mode. Thus, the interactions of microinstabilities of different types may play a non-negligible role in determining the whole properties of turbulent plasma transport. This problem has recently been addressed by direct gyrokinetic simulations that cover the ITG/TEM/ETG regimes simultaneously (see section 5.1.2). Cross-scale coupling of the ITG mode and the microscale zonal flows associated with the ETG turbulence was also discussed in an earlier work [179]. More quantitative understandings on this issue demand the use of larger computer resources as well as theoretical and/or numerical modellings relevant to simulations for the wide spatio-temporal scales.

4.2. Zonal flows and GAMs

In section 4.2.1, we describe some basic aspects of zonal flows (the turbulent-generated sheared $\boldsymbol{E}\times\boldsymbol{B}$ flows with $m = n = 0$) in ITG or ETG turbulence. An oscillating component of $\boldsymbol{E} \times \boldsymbol{B}$ flows with $n = 0$ referred to the geodesic acoustic mode (GAM), which is coupled to the zonal flows through the toroidicity, is explained in section 4.2.2. Kinetic response theory and simulations of zonal flows and GAMs in toroidal systems are also summarized in section 4.2.3.

4.2.1. Basic aspects of zonal flows. As mentioned in section 4.1.1, one of the most important findings resulting from gyrokinetic simulations of toroidal ITG turbulence is effective regulation of turbulent transport by zonal flows [6, 180]. The zonal flow is a sheared $\boldsymbol{E} \times \boldsymbol{B}$ plasma flow with poloidal and toroidal mode numbers $m = n = 0$, and is generated through the Reynolds stress in the drift wave turbulence. The radial scale length of the zonal flow shear is associated with a typical wave number range of turbulence. The zonal flow being parallel to flux surfaces causes no perpendicular heat nor particle transport. Nevertheless, it plays quite an important role in regulating turbulent transport, since sheared plasma flows can effectively suppress the microturbulence [181–183]. Thus, the self-generated zonal flow in the plasma turbulence is now recognized as a key constituent of a *drift wave-zonal flow system*.

The zonal flows are also found in nature. The most famous example is the strong longitudinal winds in the Jovian atmosphere. Early evidence of zonal flows in 2D turbulence fluid simulations was found in [184]. The zonal flow was also found by a computer simulation of resistive drift wave turbulence [185]. In simulations of ITG turbulence, the zonal flow was identified by means of local flux-tube models in the early 1990s [67, 155–158]. The increase in computer power enabled one to perform global gyrokinetic simulations of zonal flow generation in ITG turbulence at a later time [64, 70] where the proper treatment of adiabatic electron response [186, 187], $\delta n_e/n_0 = e(\phi - \langle\phi\rangle_f)/T_e$, was also implemented.

A typical result of the global ITG turbulence simulation with self-generated zonal flows is shown in figure 9(left). The ion heat transport significantly increases for the case without zonal flows (figure 9 (right)). Because of the strong reduction in the ion heat transport in the ITG turbulence, the zonal flow has attracted many researchers' attention not only in numerical simulations but also in laboratory experiments. The first identification of zonal flows in fusion plasma experiments was made by utilizing a set of heavy ion beam probes in the Compact Helical System [188]. Recent progress of zonal flow experiments is reviewed in [189].

Mechanisms of zonal flow generation have been considered as resulting from a parametric nonlinear instability through coupling of a zonal flow and coherent drift waves [190], modulational instability of a drift wave spectrum [191] and the Kelvin–Helmholtz (K–H) instability of radially elongated vortices [192]. For the saturation of zonal flow growth in turbulence, several mechanisms have been discussed, and are summarized in [6]. Generalized K–H instability is one of the candidates for a saturation mechanism of zonal flows in the ITG [192, 193] and the ETG [194, 195] turbulence.

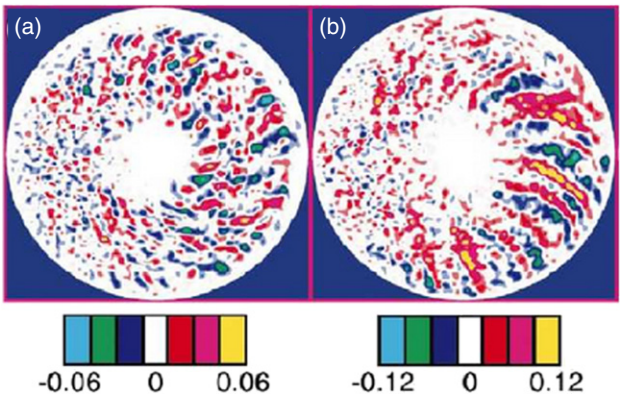

Figure 9. Colour contours of potential fluctuations found in the steady state of nonlinear global gyrokinetic simulations (*a*) with and (*b*) without zonal flows [64]. To highlight differences in the turbulent eddy size, the zonal flow component is filtered out in the plots.

Moreover, the importance of parallel flows and viscosity in the zonal flow saturation is pointed out [196].

The zonal flows are more strongly generated in the ITG turbulence than in the ETG turbulence. In the former, since the electron gyroradius is negligibly small, the adiabatic electrons cannot respond across the zonal flow potential that is constant on a flux surface. No electron density perturbation, thus, arises for the zonal flow components of $m = n = 0$, since the parallel and perpendicular motions are on the flux surface. Therefore, in the ITG regime, the electron density is modelled as $\delta n_e/n_0 = e(\phi - \langle\phi\rangle_f)/T_e$ [186, 187] where $\langle\phi\rangle_f$ means the electrostatic potential averaged on the flux surface (that is, the zonal flow potential). Hence, in the quasi-neutrality condition given by neglecting the $-\nabla^2\phi$ term in the gyrokinetic Poisson equation in equation (26), the ion density perturbation vanishes for the zonal flow component. This means that the ion gyro-centre density perturbation ($\delta\bar{n}_i$) for zonal flows balances the ion polarization (they correspond to the first and second terms in square brackets for $s = i$ in the right-hand side of equation (26)). In a long wavelength limit $k_\perp\rho_i \ll 1$, thus, $e\phi_{ZF}/T_i \propto \delta\bar{n}_i/k_\perp^2\rho_i^2 n_0$, where ϕ_{ZF} means the electrostatic potential of a zonal flow. For other perturbations with $m \neq 0$ or $n \neq 0$ such as the ITG mode, in contrast, $e\phi/T_i \propto \delta\bar{n}_i/(T_i/T_e + k_\perp^2\rho_i^2)n_0$ because of the non-vanishing electron response. This is referred to as *small inertia* of zonal flows in the ITG regime [6], and leads to the zonal flow dominant state of turbulence. In the ETG regime, the adiabatic ion response given in the large $k_\perp\rho_i$ limit can balance the zonal fluctuations of the electron density. Thus, both for the ETG mode and zonal flows, $e\phi/T_e \propto \delta\bar{n}_e/(T_e/T_i + k_\perp^2\rho_e^2)n_0$, where $\delta\bar{n}_e$ means the gyro-centre density perturbation for electrons. The different responses of the background species result in weaker generation of zonal flows and higher heat conductivity normalized in the gyro-Bohm unit for the ETG turbulence than that for the ITG case.

Zonal flows associated with the ETG mode are, therefore, less important for transport reduction than those in the ITG turbulence, but exhibit more variety, such as sensitivity to the magnetic shear [194, 195] and transition to a vortex-dominant state with the density-gradient dependence [197]. In addition, the weak zonal flow resulting in higher saturation levels of ETG turbulence causes difficulties in numerical simulations, which induces arguments on the soundness of gyrokinetic simulations of ETG modes [72, 151, 198].

4.2.2. Geodesic acoustic modes. In toroidal systems, the zonal flow is coupled to a perturbation with $m \neq 0$ and $n = 0$ which is referred to as the geodesic acoustic mode (GAM) [199]. An $\boldsymbol{E} \times \boldsymbol{B}$ plasma flow with $m = n = 0$ causes a density perturbation with $m = 1$ because of the compressibility of $\boldsymbol{E} \times \boldsymbol{B}$ flow in the non-uniform magnetic field. The ion diamagnetic current due to the $m = 1$ density perturbation transports charge across the magnetic surface, and acts to reverse the electric field [199]. Then, an oscillating component of the zonal flow potential is generated, that is, the GAM, of which real frequency ω_{GAM} is approximated by $\omega_{GAM} \simeq \sqrt{7/2 + 2(T_e/T_i)}v_{ti}/R$ for $v_{ti} = \sqrt{T_i/m_i}$. The GAM oscillations have been observed in many tokamak and helical experiments [189].

In collisionless plasmas, the GAMs are Landau damped by passing ion motions. The collisionless damping becomes ineffective for a large safety factor, as the damping rate γ_{GAM} is roughly in proportion to $\exp[-(Rq\omega_{GAM})^2/2v_{ti}^2]$ [200]. This is because the resonance velocity shifts to a tail region of the distribution function as q increases. Thus, the GAM can be prominent in edge plasmas [201]. A detailed gyrokinetic analysis of GAMs with a finite radial wavenumber effect has been made for tokamak and helical configurations [202–206] and is utilized in benchmarking of various gyrokinetic simulation codes. Plasma shaping effects on GAMs have also been investigated for a non-circular and finite aspect ratio torus [207].

The time-varying $\boldsymbol{E} \times \boldsymbol{B}$ plasma flow has been considered to be less effective in turbulence regulation than the stationary zonal flows [208]. The influence of the GAM on turbulent transport as well as its excitation process is discussed in terms of a fluid model [209]. It has also been shown that the transport suppression by zonal flows is weakened in a region where GAMs are dominant [210, 211]. In a more recent study, it is argued that the GAMs are only somewhat less effective than the residual zonal flows in providing the nonlinear saturation of turbulence [212]. The role of GAM in the turbulence regulation demands further investigations.

The GAM oscillations also appear in the neoclassical transport analysis of spontaneous formation of the radial electric field, and are studied by means of drift-kinetic equations for tokamak and helical systems [54, 200, 213, 214].

4.2.3. Zonal flow response. The generation of zonal flows and its feedback to turbulence and transport are essentially nonlinear processes. Nevertheless, it is also important to understand the linear response of zonal flows to a given turbulence. From the gyrokinetic equations, Rosenbluth and Hinton derived the zonal flow response function (kernel) which describes how strongly a zonal flow is generated by a given source term with a Maxwellian distribution [139].

The zonal flow potential is given by the response kernel $\mathcal{K}(t)$, such that

$$\phi_{\boldsymbol{k}_\perp}(t) = \mathcal{K}(t)\phi_{\boldsymbol{k}_\perp}(0), \tag{53}$$

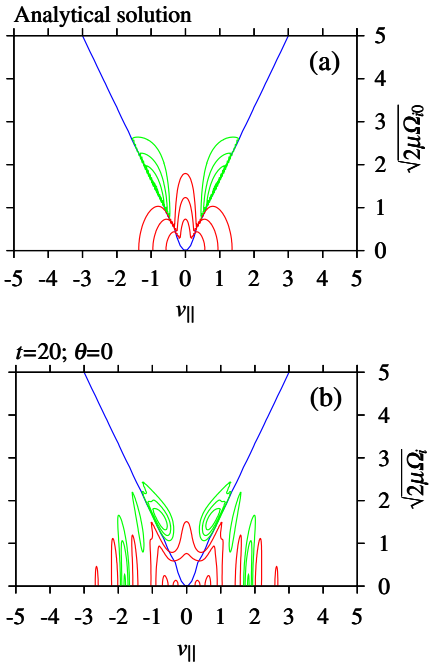

Figure 10. Velocity-space profiles of real part of the perturbed distribution functions for (*a*) the analytical solution of the residual zonal flow component and (*b*) the gyrokinetic simulation of the collisionless zonal flow damping [97]. The ion gyro-centre distribution function in (*b*) observed during the collisionless damping of zonal flows consists of the coherent structure shown in (*a*) and ballistic-mode fluctuations.

where

$$\mathcal{K}(t) = \mathcal{K}_{\rm GAM}(t)[1 - \mathcal{K}_{\rm L}(t)] + \mathcal{K}_{\rm L}(t). \qquad (54)$$

The short-time response function $\mathcal{K}_{\rm GAM}(t)$ represents the collisionless damping of GAM,

$$\mathcal{K}_{\rm GAM}(t) = \cos(\omega_{\rm GAM}t)\exp(-\gamma_{\rm GAM}t). \qquad (55)$$

The long-time response kernel $\mathcal{K}_{\rm L}(t)$ describes the residual zonal flow. For the ITG turbulence in a tokamak, it is given by [139]

$$\mathcal{K}_{\rm L} = \lim_{t\to\infty}\frac{\langle\phi_{\boldsymbol{k}_\perp}(t)\rangle_{\rm f}}{\langle\phi_{\boldsymbol{k}_\perp}(t=0)\rangle_{\rm f}} = \frac{1}{1+1.6q^2/\epsilon^{1/2}}, \qquad (56)$$

where ϵ denotes the inverse aspect ratio. The second term in the denominator in equation (56) shows effects of the neoclassical polarization on shielding of zonal flows. Velocity-space structures of distribution functions for the residual zonal flow and for the ballistic perturbations associated with the collisionless GAM damping are revealed by gyrokinetic theory and simulations [97] (see figure 10). The residual zonal flow in the collisionless ITG turbulence is also considered to provide a key for understanding the discrepancy [121] of ion heat transport flux between the gyrofluid and gyrokinetic simulations [139, 141]. Then, the zonal flow response has been regarded as a good benchmark test for gyrokinetic simulation codes (see the previous section).

In the case of finite collisionality, the residual zonal flow is slowly damped on a collisional time scale [215], while it keeps a constant value in the collisionless case as shown in equation (56). Effects of plasma shaping [216–218], kinetic electron response [219] and the zonal flow response in a wide wavenumber range including the ETG regime [220–223] have also been studied for tokamak configurations.

Figure 11. Elongated vortices (streamers) are found in contours of electrostatic potential fluctuations of toroidal ETG turbulence in a poloidal plane [95]. The horizontal axis is in the radial direction.

The Rosenbluth–Hinton theory has been generalized for helical systems by taking into account helical components of the confinement field and finite wavenumber effects [204, 205, 224–226] where, in contrast to the tokamak case, $\mathcal{K}_{\rm L}$ has time dependence and involves an additional shielding term due to radial drift motion of helical-ripple-trapped particles. Being based on the response analysis, zonal flow enhancement by reducing the neoclassical ripple transport [126, 227] or by introducing the equilibrium radial electric field [228–230] has been studied by both the gyrokinetic theory and simulations. The obtained results suggest that a coupling of anomalous and neoclassical transport appears through zonal flows in helical systems.

4.3. Radial flow and propagation

4.3.1. Streamers. Streamers, which are radially elongated vortices of the $\boldsymbol{E}\times\boldsymbol{B}$ plasma flows, are regarded as a counterpart of the zonal flows. In contrast to the latter, the former enhances the transport across the confinement field (for example see figure 9(*b*)). The linear eigenfunction of drift waves in a torus has the ballooning-type mode structure, of which the poloidal flow pattern for high (m, n) values consists of radially elongated eddies ($k_r \sim 0$). The mode structure is regarded as a *linear* streamer, and its stability to the K–H mode is investigated as one of possible mechanisms for zonal flow generation [192].

Streamers surviving in turbulence have more impact on the theory and simulations of anomalous transport. Because of the relatively weak generation of zonal flows, the streamers are expected to dominate in the ETG turbulence. The ETG streamers found in a flux-tube gyrokinetic simulation are shown in figure 11 [95]. Since the radially elongated structure suggests a long correlation length of turbulence, a strong electron heat transport is expected according to the mixing length estimate. This is why the ETG streamers have been intensively studied (see section 5.1.2).

4.3.2. Avalanches and turbulence spreading. The streamers explained above are characterized by radially elongated vortex structures. On the other hand, avalanches in density and/or temperature profiles propagate in the radial direction, where fluctuations are successively destabilized at the propagation front with steep gradients. A physical model of the avalanche is based on the self-organized criticality (SOC) of dynamical systems [231, 232], where local perturbations propagate over

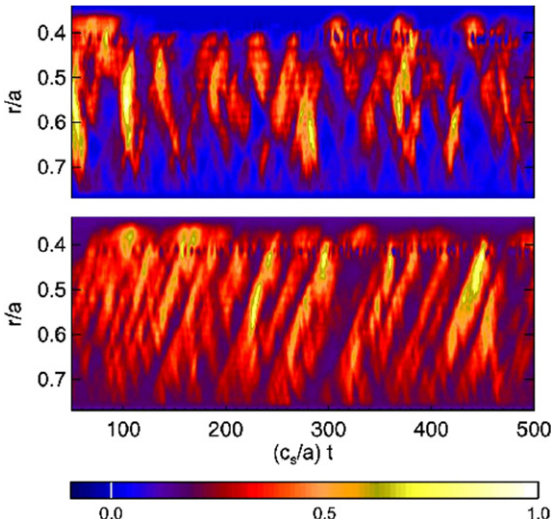

Figure 12. Heat flux avalanches with (lower) and without (upper) toroidal rotation [240]. When sheared rotation is included, avalanches of outward heat flux propagate towards the core.

all length scales surviving over long-time scales, and cause sub-critical transport. Then, noise propagation due to the *domino* effect generates $1/f$ noise in space and time with the scale invariance and the self-similarity. Avalanches in the plasma turbulent transport have been investigated by the use of reduced or low-dimensional models [233–236] or by means of direct numerical simulations [237–239], showing some analogies to the SOC model. Recent gyrokinetic simulations [58, 120, 240] also suggest avalanches of flux-surface-averaged fluctuations and/or transport flux (see figure 12). The flux driven boundary condition [238] and non-local modelling are essential to self-organization of density and temperature profiles with avalanches. The self-organized profiles found in the plasma turbulence simulations often show super-critical gradients in contrast to the original SOC model.

Turbulence spreading observed in gyrokinetic simulations [241–243] is also related to the radial propagation of perturbations [244, 245], where the turbulent fluctuations generated by the unstable drift waves enter stable regions. Because of the turbulence spreading, the averaged intensity of fluctuations is decreased in comparison with the local flux-tube model where the instability grows over the whole radial extent. Various theories have been proposed for the turbulence spreading and the front propagation [236, 242, 243, 246, 247]. These recent activities are partly motivated by a conjecture that turbulence spreading is responsible for the deviation of transport scaling from gyro-Bohm to Bohm for relatively small sized tokamaks [144]. If the radial width of spreading is independent of the device size or ρ_* ($= \rho_{ti}/a$ where a denotes the minor radius), contribution of spreading to the global confinement is weakened by decreasing ρ_*. In the limit of $\rho_* \to 0$, thus, one finds the gyro-Bohm scaling (see section 4.5). It is pointed out by recent gyrokinetic simulations that the radial extent of the spreading is influenced by an equilibrium $\boldsymbol{E} \times \boldsymbol{B}$ shear flow as well as zonal flows [68], and that non-diffusive processes are observed in turbulent transport across sheared zonal flows [248].

4.4. Fluctuations of distribution function

Microturbulence in collisionless or weakly collisional plasmas causes fluctuations of the particle distribution function in the multi-dimensional phase space. In addition to the zonal flow generation (section 4.2.1), the nonlinear $\boldsymbol{E} \times \boldsymbol{B}$ advection (or interactions among vortices) leads to the normal and/or inverse cascade of energy or enstrophy. The turbulent fluctuations are spontaneously generated not only in real space but also in velocity space through the parallel advection, the toroidal magnetic drift and the mirror force terms in the gyrokinetic equation as well as the $\boldsymbol{E} \times \boldsymbol{B}$ advection term with finite-gyroradius effect. All these terms are formally represented as

$$U(Z_i, \ldots)\frac{\partial f(Z_i, Z_j, \ldots)}{\partial Z_j}, \tag{57}$$

where Z_i and Z_j are a pair of phase space coordinates. The linear or nonlinear *shear* operator defined in equation (57) stretches the distribution function f in phase space and generates fine structures of f. Phase mixing of the fine scale fluctuations of f causes collisionless damping of *coarse-grained* quantities (that is, Landau damping). In the weakly collisional case, the small scale fluctuations in the velocity space are finally dissipated by collisions, and the irreversibility appears in the turbulent transport.

The generation processes of fine structures of f in the parallel [74, 40] and the perpendicular [249–251] velocity space have been investigated, where the production of entropy and its transfer in phase space are discussed. In a flux-tube model of ITG turbulence under fixed gradients of density and temperature, the entropy balance equation (normalized) can be simply represented as [97]

$$\frac{\mathrm{d}}{\mathrm{d}t}(\delta S + W) = \eta_\mathrm{i} Q_\mathrm{i} + D_\mathrm{i}, \tag{58}$$

where δS, W, Q_i and D_i denote the entropy variable, potential energy, ion heat transport flux and collisional dissipation, respectively. It is important to note that δS defined by means of a phase space integral of $\delta \bar{f}_\mathrm{i}^2/2 f_\mathrm{Mi}$ reflects growth of fine scale fluctuations of the distribution function. In the collisionless or weakly collisional turbulence simulations, the generation of fine scale fluctuations of f demands fine velocity-space resolution [97] or use of numerical filters [136]. Thus, the entropy balance is regarded as one of the important benchmark tests of the gyrokinetic simulation codes. Also, the entropy transfer towards small scales in velocity space is closely associated with the closure problem of fluid equations in the collisionless regime [186, 252–256].

4.5. Dimensionless scaling laws

The scaling property of turbulent transport is one of the most important topics that attract many researchers' attention in predicting the performance of fusion plasmas in future devices such as ITER. It is considered that turbulent transport is mostly related to three dimensionless parameters, the normalized ion gyroradius (ρ_*), collisionality (ν_*) and plasma pressure (β). Scaling laws for the three parameters and other dimensionless quantities have been elaborated from numerous experimental results [257].

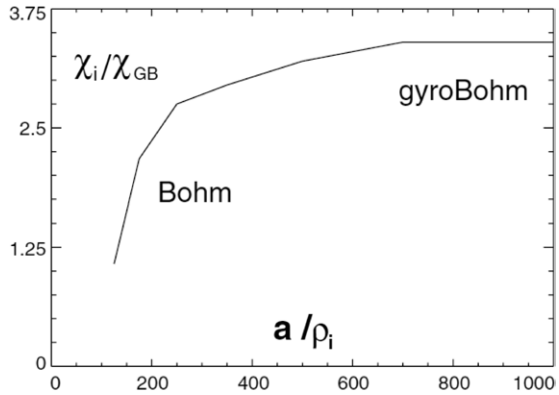

Figure 13. Dependence of ion heat conductivity on tokamak minor radius resulting from global gyrokinetic simulation of ITG turbulence [144].

For predicting the performance of ITER, the scaling for ρ_* is crucial, since the present tokamak experiments cannot achieve the expected ρ_* values of $\rho_* \simeq 2 \times 10^{-3}$ or less. If we assume the correlation length and time of turbulence to be $\rho_{\rm ti}$ and $a/v_{\rm ti}$, respectively, the thermal conductivity is estimated as

$$\chi_{\rm GB} = \rho_{\rm ti}^2/(a/v_{\rm ti}) = \rho_* T_{\rm i}/eB, \tag{59}$$

which is known as the gyro-Bohm diffusion. In contrast, one finds the Bohm diffusion of

$$\chi_{\rm B} = a\rho_{\rm ti}/(a/v_{\rm ti}) = T_{\rm i}/eB \tag{60}$$

if the radial correlation length of turbulence scales as $\sqrt{a\rho_{\rm ti}}$.

In flux-tube simulations the physical system size does not enter the formulation. More precisely, the flux-tube model is an approximation valid in the infinite system size limit, $\rho_* \to 0$. Therefore gyro-Bohm scaling is naturally obtained in such simulations, where the perpendicular wavelength and the time are normalized by $\rho_{\rm ti}$ and $a/v_{\rm ti}$ (or $L/v_{\rm ti}$ with a typical equilibrium scale L), respectively. Since the normalized $\chi_{\rm i}$ resulting from flux-tube simulations is independent of the system size, then a gyro-Bohm scaling is derived [67]. Deviation from the gyro-Bohm scaling, however, has been observed in global gyrokinetic simulations with moderate values of ρ_*. The transition from Bohm to gyro-Bohm scaling with decreasing ρ_* is confirmed by recent gyrokinetic simulations (see figure 13) [104, 119, 144]. The mechanism of the scaling transition is explained by non-local effects on turbulence, that is, the diamagnetic rotation shear (or ω_*-shear in short) due to inhomogeneous equilibrium gradients [258, 259] and the turbulence spreading (see section 4.3.2).

Finite collisionality has multiple effects on turbulent transport. The zonal flows are slowly damped by ion–ion collisions [215]. Gyrokinetic simulations indicate that collisional zonal flow damping leads to an enhancement of ITG turbulent transport even in a regime where the instability is almost collisionless [43]. A similar effect of collisions on zonal flows and transport has been confirmed by fluid simulations [44]. In contrast, collisions contribute to the stabilization of the TEM by particle de-trapping [45]. The resulting influence of the two contrasted roles of collisions on turbulent transport remains to be resolved.

Collisions are also indispensable to the realization of statistically steady states of kinetic plasma turbulence [40]. Small scale fluctuations of the distribution function generated in phase space can only be damped by collisions. It has been confirmed by slab ITG simulations scanning a wide range of collision frequencies that, in the limit of $\nu_* \to 0$, the turbulent transport with finite collisionality asymptotically approaches the collisionless result [40]. For a discussion on the numerical aspects of realizing statistically converged steady states, see section 3.3.

A scaling law for β reflects electromagnetic effects on turbulence as well as changes in equilibrium profiles (that is, the Shafranov shift of the magnetic axis position). Since a finite value of β reduces linear growth rates of the ITG instability as described in section 4.1.4, the ion heat diffusivity χ_i decreases with β below the stability limit of the KBM [219, 260, 261]. The scaling for higher β values than the KBM threshold would be more realistic to recent experiments in large tokamaks, and has recently been investigated using the GENE code, where χ_i increases above the threshold (but below the ideal MHD stability limit) [169].

Another important topic in transport scaling concerns the ion mass. A variety of isotope effects have been reported in experiments but remain to be resolved [257]. According to the gyro-Bohm scaling, $\chi_{\rm i}$ should be proportional to $A^{1/2}$, where A denotes the ion atomic mass number, while the energy confinement in experiments is sometimes improved in deuterium discharges as compared with hydrogen. (Here, it should be noted that the core transport in H-mode plasmas in JET slightly degrades with A while an improvement is observed in the edge region [262].) The influence of equilibrium $\boldsymbol{E} \times \boldsymbol{B}$ flows for different ion species may yield isotope effects through the Mach number dependence [229, 263, 264]. More elaborate simulation studies on the isotope effects should be pursued towards the prediction of turbulent transport in burning plasmas.

Other dimensionless parameters, such as the safety factor or the charge number, also play important roles in transport. The improvement of confinement with plasma current, which translates into a diffusivity that increases with the safety factor, has received several explanations based on the downshift of wave number spectra due to Landau damping [160, 265, 266], damping of GAMs [211] and finite orbit effects. The effect of charge number can be understood essentially from linear theory, and can be either stabilizing or destabilizing. Above the threshold, the stabilizing effect is dominant, and is a consequence of the dilution effect on the interchange drive [267–270].

5. Understanding turbulent transport with gyrokinetic simulations

5.1. Transport channels.

5.1.1. Ion heat transport. Ion heat transport was historically the first to be addressed by numerical simulations and can be considered mature. In fact, the computation of ion heat diffusivity has become a way of comparing codes, as discussed in section 3.4. This was done within the frame of the Cyclone project [121] and the TF-ITM IMP4 project [145]. The later

work also made a comparison of fluctuation and flux spectra. Several results came out of these exercises. First, the actual threshold was found to be larger than the linear stability threshold (Dimits shift). Second, the heat diffusivity was found to match the approximate relation $\chi_i = 12.3\chi_{i,GB}(1-6L_{Ti}/R)$ ('LLNL fit'), where L_{Ti} is the temperature gradient length. This expression illustrates the concept of profile stiffness: since transport becomes quite large above the threshold, the temperature gradient length tends to stay close to the threshold, leading to a resilience of the temperature profile. Also, heat diffusivities calculated by gyrokinetic simulations were found to be lower than the fluid values in the Cyclone exercise. In the TF-ITM project, some of the diffusivities are below the LLNL fit. Nevertheless, the same trend remains qualitatively true. Comparison with experimental data appears to be challenging. This is believed to be due to stiffness: a slight change in the gradients leads to large variations of the heat diffusivity. It is expected that the next generation of gyrokinetic codes, which will be flux driven instead of running at fixed gradient, will allow direct comparison between codes and experiments.

5.1.2. Electron heat transport. Electron heat transport is still subject to discussion. First, it is stressed that dominant ITG turbulence does lead to some amount of electron transport, which agrees with the quasi-linear prediction. Nevertheless, it is found that the corresponding contribution is too small to explain the measured diffusivity when electron heating is dominant. Hence it is expected that trapped electron modes (TEM) and/or electron temperature gradient (ETG) driven modes play some role. Gyrokinetic simulations show indeed that TEM modes contribute to electron transport above the stability threshold. The diffusivity can be fit by a formula of the LLNL type. A nonlinear upshift of the critical density gradient has been computed [159], reminiscent of the Dimits shift of the ion temperature gradient for ITG turbulence [121] (note that TEMs can be driven unstable by both density and electron temperature gradients). Nevertheless, measurements of the electron temperature gradient agree well with the linear threshold for the TEM, without any evidence of a Dimits type shift [161]. The saturation mechanism of TEM seems different from ITG modes. Whereas zonal flows are found to play a prominent role for ITG turbulence, it appears that mode coupling to small scale fluctuations, which act as diffusion, is a key ingredient for TEM turbulence. This behaviour provides some ground for applying the quasi-linear theory [162]. However, the question of saturation is not fully settled, since zonal flows, and also profile relaxation play a role in some cases [163, 164].

The question of ETG driven turbulence has been, and still is, a very active subject. If one assumes an homothetic behaviour to ITG turbulence, a gyro-Bohm estimate predicts an electron diffusion coefficient that is $(m_e/m_i)^{1/2}$ smaller than the ion heat diffusivity. Since the measured electron diffusion coefficient is of the same order as the ion value, it appears that the expected value for ETG turbulence is too small by an order of magnitude. However, it was realized in [93, 95] that zonal flows are less efficiently generated in ETG than in ITG turbulence, because the adiabatic responses of ions (in ETG) and electrons (in ITG) are different. A smaller intensity of zonal flows in ETG turbulence favours the emergence of streamers, which may boost the heat transport. It was found indeed that zonal flows play little role in the saturation of ETG modes, rather due to wave–particle decorrelation [165]. Because of their central importance in that matter, streamers have been studied intensively. Although there is agreement on their existence, the enhancement factor associated with streamers varies somewhat in the literature [149, 195]. Certainly the magnetic shear plays an important role in that matter: streamers tend to be dominant for high magnetic shear, while zonal flows are dominant at low shear [95, 197, 271] (see figure 14). Also, it turns out that numerical issues make the exercise difficult, as was discussed in section 3.4. It was also mentioned that ETG turbulence with adiabatic ions is sometimes an ill-posed problem due to the interaction with TEMs at low wave numbers [150, 272]. A similar large-saturation problem was reported also for ITG with kinetic electrons [273]. A key step was reached with simulations done with the GYRO code covering the whole spectrum of instabilities (ITG, TEM, ETG). In these simulations, it was found that the contribution of large wave numbers $k_\perp\rho_i > 1$ to the electron diffusivity is less than 15% in a typical case where electron and ion temperature gradient lengths are equal [272] (see figure 15, upper panel). This was confirmed by a recent simulation with the GENE code where a comparable figure was found in similar conditions [273]. However, it was also mentioned in the latter work that the parameters that were chosen correspond to a very large, and unrealistic, ion heat transport. In the same work, it is also shown that when the electron temperature gradient length is smaller than the ion temperature gradient length (and also for a vanishing density gradient), small scales contribute significantly to electron turbulent transport, while the ion heat diffusivity gets closer to experimental values (see figure 15, lower panel).

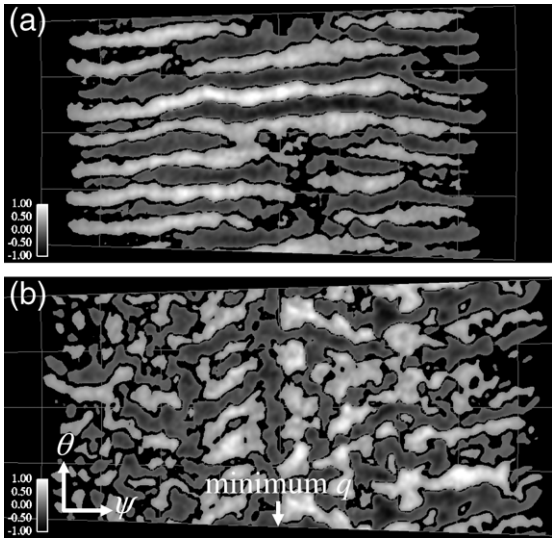

Figure 14. Contour plots of the electric potential in ETG turbulence for simulations with (*a*) positive magnetic shear, dominated by streamers and (*b*) reversed magnetic shear dominated by zonal flows (from [271]).

5.1.3. Particle transport. Particle transport is obviously an important question for a fusion reactor. On the one hand, one

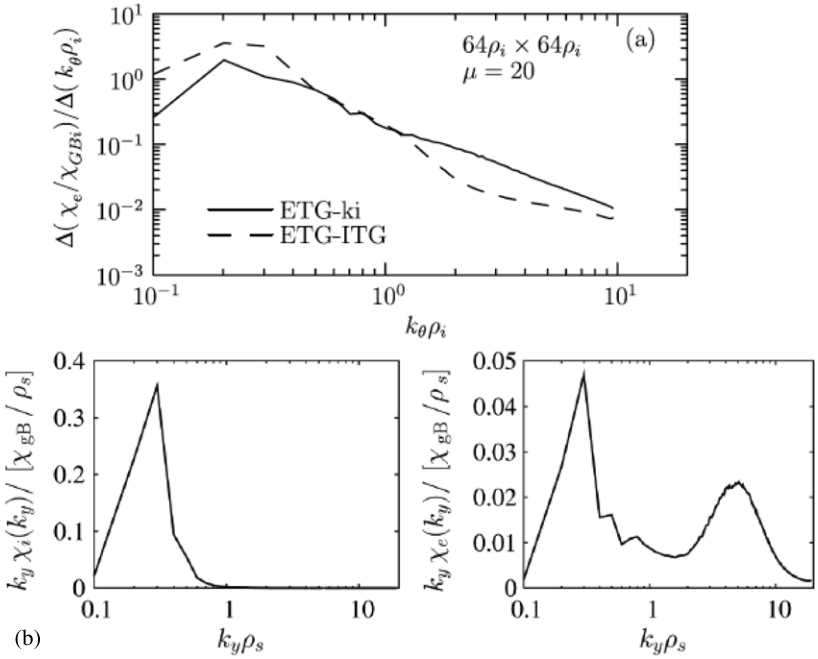

Figure 15. Upper panel: simulations of ITG/TEM/ETG turbulence with the GYRO code for equal electron and ion temperature gradient length $R/L_{T_i} = R/L_{T_e} = 6.89$ and $R/L_{n_e} = 2.22$ [272]. Lower panel: simulations with the GENE code of ITG/ETG/TEM turbulence for electron temperature gradient length smaller than the ion gradient length, i.e. $R/L_{T_i} = 5.5$, $R/L_{T_e} = 6.9$ and $R/L_{n_e} = 0$—ion heat diffusivity on the left, electron heat diffusivity on the right [273].

would like the density to be as high as possible to enhance the fusion power. Since the edge density must remain low enough to avoid a disruption (Greenwald limit), peaked density profiles are desirable. On the other hand, peaked density profiles might lead to neoclassical impurity accumulation in the core. One key characteristic of the particle flux is that it is not correctly described by a pure diffusion. Indeed it is well known that density profiles are peaked, even when the ionization source is localized in the edge. To account for this behaviour, the particle flux is traditionally written as $\Gamma = -D\nabla n + Vn$ [274–276], where V is the pinch velocity and D is the particle diffusion coefficient. Fluid and gyrokinetic simulations (quasi-linear and fully nonlinear) indeed show that a finite pinch velocity is driven by turbulence. This velocity contains 'curvature' (or 'compressional') and thermodiffusion contributions, i.e. schematically $\frac{VR}{D} = C_{\rm curv} + C_{\nabla T} R\frac{\nabla T}{T}$ [277–279]. The coefficient $C_{\rm curv}$ is related to compressional effects and is well described by turbulence equipartition theory [280, 281]. It can be shown that when trapped electrons behave as trace particles in a dominant ITG turbulence, one gets $C_{\rm curv} = 1/2 + 4s/3$ ($s = {\rm d}\ln q/{\rm d}\ln r$ is the magnetic shear). Hence the curvature pinch introduces a link between the density and safety factor profiles. However, it was also shown that passing electrons also participate in the pinch process [282]. The thermodiffusion coefficient $C_{\nabla T}$ can be shown to change sign with the phase velocity of fluctuations, i.e. when moving for instance from ITG to TEM turbulence [278, 279]. Typically, the thermal pinch velocity is directed outwards ($C_{\nabla T} < 0$) for ITG turbulence. Collisionality plays an important role in that matter. Indeed the ratio VR/D, which is representative of the peaking factor of the density, decreases as $1/\nu_*$ [283].

A related question is the issue of impurity transport. In that case again, a pinch velocity is driven by turbulence. Here it is found that the thermodiffusion coefficient is directed outwards for ITG turbulence, which is favourable (thermal screening). Unfortunately the coefficient of the thermodiffusion term decreases as $1/Z$, where Z is the charge number [284, 285]. Hence it is negligible for heavy impurities. The compressional term contains two contributions due to perpendicular and parallel compressibility [284]. The pinch velocity associated with perpendicular compressibility is constant and directed inwards, while the one associated with parallel compressibility scales as Z/A, and its sign depends on the phase velocity of the fluctuations. It is outward for dominant TEM turbulence. Gyrokinetic simulations are roughly in agreement with the quasi-linear picture [286], although a more quantitative assessment of the dependence on charge and mass numbers is needed. This global picture of particle transport predicts non-flat density profiles in ITER, without impurity accumulation [287]. Let us also mention that the transport of alpha particles also belongs to this category. Large orbit widths are known to have a detrimental impact on the collisional transport of fast ions. On the other hand, finite orbit widths are favorable with respect to turbulent transport since fast particles 'see' an orbit-averaged electromagnetic field that gets smaller when the orbit size becomes larger than a typical correlation length. However, theoretical considerations suggest that fast ion fluxes might be larger than expected on the basis of this simple picture [288]. Gyrokinetic simulations indicate that though significant, losses remain reasonable [175, 289–291], and probably acceptable in ITER plasmas.

5.1.4. Toroidal momentum transport. Toroidal momentum transport has been investigated in detail only quite recently. These studies were motivated by the discovery of plasma 'spontaneous' spin-up, i.e. situations where a significant

toroidal rotation was measured, in the absence of any external torque (see [292] for an overview). Moreover, in many cases co-rotation was observed (toroidal velocity in the same direction as the current), which cannot be explained by simple effects such as ripple losses or direct losses of ions at the edge. The theoretical question of momentum transport is quite difficult to address. One first obstacle is actually to define properly 'momentum transport'. One would be tempted to look into the conservation of angular momentum density. However, the latter depends on particle density, which was seen to be subject to various pinch effects. In order to decouple particle and 'true' momentum pinches, it is common to investigate the transport of parallel velocity $U_\parallel$. The quasi-linear theory predicts a radial flux of parallel velocity $\Gamma_U/n_i m_i = -\chi_U \nabla U_\parallel + V_U U_\parallel + S_U$ [146, 293–299]. When compared with the expression for particle transport, an extra term S_U appears, called residual stress, proportional to the $\boldsymbol{E} \times \boldsymbol{B}$ shearing rate [293–295, 300] or due to up–down asymmetries of the equilibrium [301]. The angular momentum density can be expressed as a function of the parallel velocity, density and temperature derivatives when using the force balance equation. There exist two ways of deriving the various contributions. One solution consists in writing the equations in the frame of reference of the plasma, which requires accounting for the Coriolis and centrifugal forces (the centrifugal force is in practice negligible) [146]. The second way consists in writing the gyrokinetic equations in the laboratory frame, accounting for the fact that the distribution function is shifted in the parallel direction by an inhomogeneous mean velocity [302]. The normalized pinch velocity RV_U/χ_U contains two contributions: a constant term (this scaling is similar to the curvature pinch for particle transport) and a term proportional to the density (possibly temperature) gradient [146, 297]. The part of the pinch velocity related to curvature that is calculated in the frame of the quasi-linear theory is consistent with the turbulence equipartition theory [303, 304]. Gyrokinetic simulations did find evidence of a momentum pinch velocity and residual stress [300, 304, 305]. Another important parameter is the Prandtl number (ratio of viscosity χ_U to heat diffusivity χ_i). This ratio is usually found to be of the order 0.7 [296]. Recent simulations indicate that it can be as low as 0.2 in some cases [306]. In other words, it is found that high peaking factors RV_U/χ_U are due to both finite values of the pinch velocity V_U and low values of the viscosity χ_U. Work is actively being done to determine the relative weights of the various mechanisms at play. We note that the standard gyrokinetic ordering addresses toroidal velocities of the order of $\rho_* v_\mathrm{ti}$ (toroidal diamagnetic velocities), i.e. cannot address sonic flows, for which an extended gyrokinetic theory is needed. Obviously, this is related to the question of calculating the mean radial electric field and its shear rate, addressed in section 2.3. Diamagnetic toroidal flows correspond to values of the shear rate of the order of $\rho_* v_\mathrm{ti}/L_T$. However turbulence quench requires larger shear rates, of the order of v_ti/L_T. Solving this question would also call for an extended gyrokinetic theory.

5.2. Improved confinement

The physics of transport barriers is a broad subject that is already covered by several overview papers for external [307–310] and internal transport barriers [311–313]. Two generic key parameters are known to play a stabilizing role: flow shear and magnetic shear. Other ingredients may be involved (density gradient, ratio of electron to ion temperature, impurity content, etc), but are less generic.

5.2.1. Shear flow stabilization. The physics of turbulent transport reduction due to $\boldsymbol{E} \times \boldsymbol{B}$ shear flow is well documented. The interested reader might consult overviews on theory [183] and experiments related to shear flow stabilization [314]. Stabilization is obtained above a critical value of the shear flow rate. Several criteria have been proposed and tested [156, 181, 182, 315], which confirm the stabilizing effect of shear flows except in a few well identified cases [316]. The radial electric field is constrained by the ion force balance equation $ne(\boldsymbol{E}+\boldsymbol{V}\times\boldsymbol{B}) - \nabla p = 0$. Once a barrier is formed, a positive loop takes place where density and ion temperature gradients increase, thus boosting the velocity shear rate. The transition to improved confinement bears some similarity to first order phase transition [317–320]. Shear flow stabilization has been tested with fluid and gyrokinetic simulations. One difficulty, however, is that most gyrokinetic codes do not calculate self-consistently the mean radial electric field. A new generation of codes is emerging, which aim at this objective [57, 134, 321–323]. These codes are global, and calculate the full distribution function. This is a demanding task as it requires the calculation of the full neoclassical equilibrium as well as the turbulent generation of flow. A related question is the generation of a strong poloidal shear flow when an internal transport barrier is produced.

5.2.2. Effect of the magnetic topology. Negative magnetic shear and high values of β are known to decrease the interchange drive [324]. The effect of β is related to the Shafranov shift of magnetic surfaces (also called the α effect, $\alpha = -q^2 R\, \mathrm{d}\beta/\mathrm{d}r$ is a measure of the Shafranov shift) [325–327]. In fact this effect has long been known in the context of MHD stability [324, 328, 329]). For trapped electron modes, stabilization occurs when $s < -3/8$, while for ITG modes the exact value depends on the poloidal structure of modes. This stabilization scheme has been tested both in fluid and kinetic simulations. An electron transport barrier appears when the magnetic shear is negative [330]. This effect is amplified for values of α the order of unity. For trapped electron modes, theory predicts stability when $s < 3\alpha/5 - 3/8$. A similar effect exists for ITG modes, which comes from the shear dependence of the ion curvature averaged over the mode structure. However, it is important to note that slab ITG modes are not sensitive to these effects, and remain unstable at negative magnetic shear. One intriguing mystery is the reason why the onset of internal transport barriers appears to be easier when the magnetic shear is zero and the minimum value of the safety factor is a low order rational number. Three types of explanations have been proposed:

(i) the onset of a large scale coherent structure which acts on turbulence. This can be an MHD mode located at a rational value of q that generates a localized velocity shear [331]. An alternative explanation is based on a loss of fast ions due to MHD that leads to a shear flow [332]. More

recently, it has been proposed that a coherent electrostatic convective cell is generated and reduces transport by tapping energy on turbulence [333].

(ii) generation of zonal flows [334, 335] or GAMs [336] close to rational q values.

(iii) the existence of gaps in the density of magnetic resonant surfaces at low magnetic shear, which are wider when $q_{\min}$ is close to a low order rational number [335, 337–341].

It is stressed, however, that only a few of the aforementioned works were done with gyrokinetic simulations (mainly [335, 338]). No clear special role of $s = 0$ was found in simulations of ITG turbulence with adiabatic electrons [342], which means that more physics might have to be accounted for to describe configurations with $s = 0$, e.g. non-adiabatic electrons. Indeed the response of passing electrons is highly non-adiabatic in the vicinity of resonant surfaces [78, 168, 343]. This feature is likely a key element in the development of transport barriers. Hence this subject remains largely open to further investigation.

Shaping effects also play a role via a direct effect on the growth rate, or by affecting the dynamics of zonal flows and GAMs. Indeed the GAM frequency decreases with the elongation. Hence the damping rate of GAMs, which should lead to less active GAMs when elongation increases [344]. Also it is found that the residual Rosenbluth–Hinton flow increases with elongation [221, 344]. One might infer that in the nonlinear regime, this will lead to a higher level of zonal flows and a better confinement. Recent gyrokinetic simulations confirm this behaviour [217, 218].

5.3. Comparison with fluctuation measurements

The direct comparison of gyrokinetic simulations with fluctuation measurements is still in its infancy. One difficulty is that very few diagnostics provide turbulent fluxes, since the latter require both the advected field fluctuations (density for particle flux and temperature for heat flux), the $\boldsymbol{E} \times \boldsymbol{B}$ velocity fluctuations and their cross-correlation. So the emphasis has been put on the role of flows (zonal flows and GAMs) and turbulence, and also on the statistical properties of density, potential or temperature fluctuations. Regarding the role of zonal flows and GAMs, it turns out that theory was ahead of experiments. An early theoretical work emphasized the particular frequency signature of these modes, and also the distinction between the quasi-steady zonal flows and finite frequency GAMs [345]. Indeed zonal flows and GAMs were identified experimentally first via their frequency spectrum and then via their characteristic wave numbers $n = 0$ [188, 346–349] (see also the cluster issue on 'Experimental studies of zonal flow and turbulence' [350]). An important step was also the use of a cross bicoherence method to evidence zonal flows driven by turbulence via nonlinear mode coupling [351]. This technique was recently extended to assess the role of GAMs in the energy transfer between different scales, which was evidenced by comparing the bicoherence spectrum of beam emission spectroscopy (BES) fluctuations with GYRO simulations [352]. It was shown that GAMs are responsible for a transfer of energy from low- to high-frequency density fluctuations in the edge. A similar study remains to be done in the core. Regarding the level of density fluctuations, one of the first attempts with the GS2 code found that the predicted density fluctuation amplitude $\delta n/n_0$ was 3 times larger than the measured value with BES in DIII-D, and the simulation ion transport power was also about 2 times too large. These discrepancies would be eliminated if the temperature gradient was reduced by ∼20–33%, though it was concluded that this was outside the error bars [353]. Subsequent attempts were more encouraging. A fair agreement was found in the plasma core between measurements and simulations, whenever the measurements were done with BES in DIII-D [354], phase contrast imaging on Alcator C-Mod [355], or reflectometry on Tore Supra [356]. However, simulations tend to overestimate the level of electron temperature fluctuations when compared with correlation ECE measurements in DIII-D [357]. The situation is less satisfactory in the edge, where discrepancies between simulations and measurements are usually found [354, 357]. Comparing absolute levels of fluctuations is instructive, but the analysis of the spatio-temporal properties of fluctuations is even more interesting. Spectra have been calculated with the GENE code [358] for ITG/TEM/ETG turbulence and compared with measurements made on Tore Supra with a CO_2 laser scattering diagnostic [359]. Although encouraging, this comparison is not conclusive yet. More recently, GYRO simulations have been compared with an extensive set of measurements on TORE SUPRA based on fast-sweeping and Doppler reflectometry. A fair agreement is found for both the poloidal and radial spectra of density fluctuations [356].

6. Conclusion

Hopefully this overview has convinced the reader that the theory of turbulent transport has made enormous progress. These findings owe a lot to state-of-the-art gyrokinetic simulations which incorporate a large number of ingredients, in particular effects such as particle trapping, Landau resonances and finite orbit effects. An important step was the derivation of conservative gyrokinetic equations, which can be written at all orders in the small expansion parameter (normalized gyroradius). This effort, which involves many theoreticians and code developers, has allowed the clarification of a number of issues, such as dimensionless scaling laws, parametric dependences of the various transport channels, and improved confinement. The predicted turbulence intensities and fluxes are now getting close to the observed values. Also the processes leading to self-organization are better understood. Still several issues remain open. In particular, no first principle simulation has been able to reproduce a transition to a transport barrier, external or internal. Moreover, the comparison of simulations with experiments suffers from the sensitivity of transport to the distance of gradients to stability thresholds (stiffness). A slight mismatch in the gradients leads to a large change in fluxes, which makes this comparison very difficult. Finally, transport transients (pulses, heat modulation) have not been simulated yet, whereas these experiments are known to find puzzling results. Solving this class of problems requires simulation times of the order of the confinement time, which has not been done yet for ITER-size plasmas with gyrokinetic codes. This requirement is consistent with the long

simulations times which are necessary to reach a statistical steady state that accounts for the bursty nature of turbulent transport.

These limitations naturally lead to a discussion of the future developments. To simulate transitions to transport barriers, the next generation of gyrokinetic codes, which is emerging now, will have to calculate the full distribution function over the whole torus. This is a very difficult task, as it requires calculating both the equilibrium quantities and fluctuations, which are tiny. Also the implementation of boundary conditions is a formidable task, in particular in the edge plasmas if one wants to describe correctly the scrape-off layer and the pre-sheath and sheath close to the divertor target plates. Regarding the comparison with experiments, it also appears that the new code generation will have to be flux driven, instead of freezing gradients. This should, in principle, solve the problem of stiffness. The question of simulating both steady state and transients is even trickier. Indeed it is not foreseen at the moment to run routinely gyrokinetic codes over a confinement time and for plasmas of the ITER size—the requested computing time is indeed enormous. Presently the strategy relies on the use of reduced models [265, 277, 360, 361]. This methodology will probably remain unchanged for some time. The development of reduced transport models has made progress, in parallel with the increasing accuracy of gyrokinetic simulations. Still most models are far from being accurate enough. Although the further improvement of these models is certainly an option, one might hope that the progress in massively parallelized computation will one day allow a direct gyrokinetic calculation turbulent transport over times longer than a confinement time. An intermediate solution, recently attempted [362, 363], consists in coupling a transport code to a local gyrokinetic turbulence code, which computes the transport coefficients at several radius. Hence the coming years will certainly prove to be very interesting regarding the various challenges which remain to be solved.

Acknowledgments

The authors thank Drs P. Angelino, C. Angioni, S. Benkadda, C. Bourdelle, A. Brizard, S. Brunner, J. Candy, P.H. Diamond, G. Dif-Pradalier, G. Falchetto, P. Ghendrih, O.D. Gürcan, T.S. Hahm, G.W. Hammett, K. Itoh, F. Jenko, Z. Lin, C. Nguyen, M. Ottaviani, A.G. Peeters, Y. Sarazin, H. Sugama and R.E. Waltz for carefully reading the manuscript and making useful comments. Two of the authors (XG and LV) were partly supported by the European Communities under the contracts of Association between EURATOM and CEA (XG) and between EURATOM and Switzerland (LV), respectively, within the framework of the European Fusion Development Agreement. The views and opinions expressed herein do not necessarily reflect those of the European Commission.

References

[1] Tang W.M. and Chan V.S. 2005 *Plasma Phys. Control. Fusion* **47** R1
[2] Idomura Y., Watanabe T.-H. and Sugama H. 2006 *C. R. Physique* **7** 650
[3] Villard L. *et al* 2004 *Plasma Phys. Control. Fusion* **46** B51
[4] Ichimaru S. 1992 *Statistical Plasma Physics vol I: Basic Principles* (Redwood City, CA: Addison-Wesley)
[5] Brizard A.J. and Hahm T.S. 2007 *Rev. Mod. Phys.* **79** 421
[6] Diamond P.H. *et al* 2005 *Plasma Phys. Control. Fusion* **47** R35
[7] Frieman E.A. and Chen L. 1982 *Phys. Fluids* **25** 502
[8] Lee W.W. 1983 *Phys. Fluids* **26** 556
[9] Littlejohn R.G. 1979 *J. Math. Phys.* **20** 2445
[10] Littlejohn R.G. 1981 *Phys. Fluids* **24** 1730
[11] Littlejohn R.G. 1982 *J. Math. Phys.* **23** 742
[12] Littlejohn R.G. 1983 *J. Plasma Phys.* **29** 111
[13] Dubin D.H.E. *et al* 1983 *Phys. Fluids* **26** 3524
[14] Hahm T.S., Lee W.W. and Brizard A. 1988 *Phys. Fluids* **31** 1940
[15] Hahm T.S. 1988 *Phys. Fluids* **31** 2670
[16] Brizard A.J. 1989 *J. Plasma Phys.* **41** 541
[17] Cary J.R. 1981 *Phys. Rep.* **79** 129
[18] Cary J.R. and Littlejohn R.G. 1983 *Ann. Phys.* **151** 1
[19] Brizard A.J. 1995 *Phys. Plasmas* **2** 459
[20] Hahm T.S. 1996 *Phys. Plasmas* **3** 4658
[21] Hahm T.S., Wang L. and Madsen J. 2009 *Phys. Plasmas* **16** 022305
[22] Qin H. *et al* 2006 *Contrib. Plasma Phys.* **46** 477
[23] Qin H. Cohen R. H., Nevins W.M. and Xu X.Q. 2007 *Phys. Plasmas* **14** 056110
[24] Kawamura G. and Fukuyama A. 2008 *Phys. Plasmas* **15** 042304
[25] Artun M. and Tang W.M. 1994 *Phys. Plasmas* **1** 2682
[26] Sugama H. and Horton W. 1998 *Phys. Plasmas* **5** 2560
[27] Wang S. 2001 *Phys. Rev.* E **64** 056404
[28] Sugama H. 2000 *Phys. Plasmas* **7** 466
[29] Fong B.H. and Hahm T.S. 1999 *Phys. Plasmas* **6** 188
[30] Brizard A.J. 2000 *Phys. Plasmas* **7** 3238
[31] Kadomtsev B.B. and Pogutse O.P. 1970 *Reviews of Plasma Physics, Turbulence in Toroidal Systems* vol 5 (New York: Consultants Bureau) chapter 2
[32] Mikhailovskii A.B. 1974 *Theory of Plasma Instabilities vol 2: Instabilities of an Inhomogeneous Plasma* (New York: Consultants Bureau)
[33] Tang W.M. 1978 *Nucl. Fusion* **18** 1089
[34] Horton W. 1999 *Rev. Mod. Phys.* **71** 735
[35] Tokuda S., Naitou H. and Lee W.W. 1998 *J. Plasma Fusion Res.* **74** 44
[36] Brizard A.J. 2000 *Phys. Rev. Lett.* **84** 5768
[37] Lee W.W. and Tang W.M. 1988 *Phys. Fluids* **31** 612
[38] Krommes J.A. and Hu G. 1994 *Phys. Plasmas* **1** 3211
[39] Sugama H. *et al* 1996 *Phys. Plasmas* **3** 2379
[40] Watanabe T.-H. and Sugama H. 2004 *Phys. Plasmas* **11** 1476
[41] Hinton F.L. and Hazeltine R.D. 1976 *Rev. Mod. Phys.* **48** 239
[42] Helander P. and Sigmar D.J. 2002 *Collisional Transport in Magnetized Plasmas* (Cambridge: Cambridge University Press)
[43] Lin Z. *et al* 1999 *Phys. Rev. Lett.* **83** 3645
[44] Falchetto G.L. and Ottaviani M. 2004 *Phys. Rev. Lett.* **92** 025002
[45] Rewoldt G. and Tang W.M. 1990 *Phys. Fluids* B **2** 318
[46] Rosenbluth M.N., MacDonald W.M. and Judd D. 1957 *Phys. Rev.* **107** 1
[47] Hirshman S.P. and Sigmar D.J. 1976 *Phys. Fluids* **19** 1532
[48] Garbet X. *et al* 2009 *Phys. Plasmas* **16** 062503
[49] Brizard A.J. 2004 *Phys. Plasmas* **11** 4429
[50] Catto P.J. and Tsang K.T. 1977 *Phys. Fluids* **20** 396
[51] Xu X. and Rosenbluth M.N. 1991 *Phys. Fluids* B **3** 627
[52] Abel I.G. *et al* 2008 *Phys. Plasmas* **15** 122509
[53] Wang W.X., Hinton F.L. and Wong S.K. 2001 *Phys. Rev. Lett.* **87** 055002
[54] Satake S. *et al* 2005 *Nucl. Fusion* **45** 1362
[55] Sarazin Y. *et al* 2008 *Proc. 22nd Int. Conf. (Geneva, Switzerland, 2008)* (Vienna: IAEA) CD-ROM file

TH/P8-46 and http://www-naweb.iaea.org/napc/physics/FEC/FEC2008/html/index.htm
[56] Xu X.Q. 2008 *Phys. Rev.* E **78** 029901
[57] Heikkinen J.A. *et al* 2008 *J. Comput. Phys.* **227** 5582
[58] Idomura Y., Urano H., Aiba N. and Tokuda S. 2009 *Nucl. Fusion* **49** 065029
[59] Rosenbluth M.N. *et al* 1972 *Proc. 4th Int. Conf. on Plasma Physics and Controlled Nuclear Fusion Research 1971 (Madison, WI, 1971)* vol I (Vienna: IAEA) p 495
[60] Parra F.I. and Catto P.J. 2008 *Plasma Phys. Control. Fusion* **50** 065014
[61] Dimits A.M. 1993 *Phys. Rev.* E **48** 4070
[62] Beer M.A., Cowley S.C. and Hammett G.W. 1995 *Phys. Plasmas* **2** 2687
[63] Birdsall C.K. and Langdon A.B. 2004 *Plasma Physics via Computer Simulation (IOP Series in Plasma Physics)* (London: Taylor and Francis)
[64] Lin Z., Hahm T.S., Lee W.W., Tang W.M. and White R.B. 1998 *Science* **281** 1835
[65] Idomura Y., Tokuda S. and Kishimoto Y. 2003 *Nucl. Fusion* **43** 234
[66] Jolliet S. *et al* 2007 *Comput. Phys. Commun.* **177** 409
[67] Dimits A.M., Williams T.J., Byers J.A. and Cohen B.I. 1996 *Phys. Rev. Lett.* **77** 71
[68] Wang W.X. *et al* 2007 *Phys. Plasmas* **14** 072306
[69] Parker S.E and Lee W.W. 1993 *Phys. Fluids* B **5** 77
[70] Sydora R.D., Decyck V.K. and Dawson J.M. 1996 *Plasma Phys. Control. Fusion* **38** A281
[71] Aydemir A.Y. 1994 *Phys. Plasmas* **1** 822
[72] Nevins W.M., Hammett G.W., Dimits A.M., Dorland W. and Shumaker D.E. 2005 *Phys. Plasmas* **12** 122305
[73] Bottino A. *et al* 2007 *Phys. Plasmas* **14** 010701
[74] Watanabe T.H. and Sugama H. 2002 *Phys. Plasmas* **9** 3659
[75] Idomura Y., Ida M., Tokuda S. and Villard L. 2007 *J. Comput. Phys.* **226** 244
[76] Jolliet S. *et al* 2009 *Phys. Plasmas* **16** 052307
[77] Hatzky R., Tran T.M., Könies A. and Kleiber R. 2002 *Phys. Plasmas* **9** 898
[78] Villard L. *et al* 2004 *Nucl. Fusion* **44** 172
[79] Tajima T. and Perkins F.W. 1983 *Proc. 1983 Sherwood Theory Meeting (University of Maryland, Arlington, VA, 1983)* paper 2P9
[80] Kotschenreuther M. 1988 *Bull. Am. Phys. Soc.* **33** 2107
[81] Dimits A.M. and Lee W.W. 1993 *J. Comput. Phys.* **107** 309
[82] Allfrey S.J. and Hatzky R. 2003 *Comput. Phys. Commun.* **154** 98
[83] Manuilskiy I. and Lee W.W. 2000 *Phys. Plasmas* **7** 1381
[84] Lee W.W., Lewandowski J.L.V., Hahm T.S. and Lin Z. 2001 *Phys. Plasmas* **8** 4435
[85] Chen Y. and Parker S.E. 2003 *J. Comput. Phys.* **189** 463
[86] Hatzky R., Könies A. and Mishchenko A. 2007 *J. Comput. Phys.* **225** 568
[87] Lin Z. and Chen L. 2001 *Phys. Plasmas* **8** 1447
[88] Mishchenko A. *et al* 2008 *Phys. Plasmas* **15** 112106
[89] Metropolis N., Rosenbluth A.W., Rosenbluth M.N., Teller A.H. and Teller E. 1953 *J. Chem. Phys.* **21** 1087
[90] Courant R., Friedrichs K. and Lewy H. 1928 *Math. Ann.* **100** 32
[91] Courant R., Friedrichs K. and Lewy H. 1967 *IBM J. Res. Dev.* **11** 215
[92] Kotschenreuther M., Rewoldt G. and Tang W.M. 1995 *Comput. Phys. Commun.* **88** 128
[93] Dorland W., Jenko F., Kotschenreuther M. and Rogers B.N. 2000 *Phys. Rev. Lett.* **85** 5579
[94] Candy J. and Waltz R.E. 2003 *J. Comput. Phys.* **186** 545
[95] Jenko F., Dorland W., Kotschenreuther M. and Rogers B.N. 2000 *Phys. Plasmas* **7** 1904
[96] Merz F. 2008 Gyrokinetic simulation of multimode plasma turbulence *PhD Thesis* Münster University
[97] Watanabe T.H. and Sugama H. 2006 *Nucl. Fusion* **46** 24
[98] Peeters A.G. and Strinzi D. 2004 *Phys. Plasmas* **11** 3748
[99] Idomura Y., Ida M., Kano T., Aiba N. and Tokuda S. 2008 *Comput. Phys. Commun.* **179** 391
[100] Filbet F., Sonnendrücker E. and Bertrand P. 2001 *J. Comput. Phys.* **172** 166
[101] Morinishi Y., Vasilyev O.V. and Ogi T. 2004 *J. Comput. Phys.* **197** 686
[102] Brunetti M., Grandgirard V., Sauter O., Vaclavik J. and Villard L. 2005 *Comput. Phys. Commun.* **163** 1
[103] Grandgirard V. *et al* 2006 *J. Comput. Phys.* **217** 395
[104] Grandgirard V. *et al* 2007 *Plasma Phys. Control. Fusion* **49** B173
[105] Brunetti M. *et al* 2005 *Transport Theor. Stat. Phys.* **34** 333
[106] Suresh A. and Huynh H.T. 1997 *J. Comput. Phys.* **136** 83
[107] Collela P. and Sekora M.D. 2008 *J. Comput. Phys.* **227** 7069
[108] Dimits A.M. and Cohen B.I. 1994 *Phys. Rev.* E **49** 709
[109] Boozer A.H. and Kuo-Petravic G. 1981 *Phys. Fluids* **24** 851
[110] Lin Z., Tang W.M. and Lee W.W. 1995 *Phys. Plasmas* **2** 2975
[111] Wang W.X., Nakajima N., Okamoto M. and Murakami S. 1999 *Plasma Phys. Control. Fusion* **41** 1091
[112] Lin Z., Hahm T.S. and Lee W.W. 2000 *Phys. Plasmas* **7** 1857
[113] Brunner S., Valeo E. and Krommes J.A. 1999 *Phys. Plasmas* **6** 4504
[114] Chen Y. and White R.B. 1997 *Phys. Plasmas* **4** 3591
[115] Lewandowski J.L.V. 2005 *Phys. Plasmas* **12** 052322
[116] Lederer H., Tisma R., Hatzky R., Bottino A. and Jenko F. 2008 *Advances in Parallel Computing* vol 15 (Amsterdam: IOS Press) p 713
[117] Kim C.C. and Parker S.E. 2000 *J. Comput. Phys.* **161** 589
[118] Hatzky R. 2006 *Parallel Comput.* **32** 325
[119] Candy J., Waltz R.E. and Dorland W. 2004 *Phys. Plasmas* **11** L25
[120] McMillan B.F. *et al* 2009 *Phys. Plasmas* **16** 022310
[121] Dimits A.M. *et al* 2000 *Phys. Plasmas* **7** 969
[122] Miller R.L., Chu M.S., Greene J.M., Lin-Liu Y.R. and Waltz R.E. 1998 *Phys. Plasmas* **5** 973
[123] Lütjens H., Bondeson A. and Sauter O. 1996 *Comput. Phys. Commun.* **97** 219
[124] Jenko F. and Kendl A. 2002 *Phys. Plasmas* **9** 4103
[125] Xanthopoulos P., Merz F., Görler T. and Jenko F. 2007 *Phys. Rev. Lett.* **99** 035002
[126] Watanabe T.H., Sugama H. and Ferrando-Margalet S. 2008 *Phys. Rev. Lett.* **100** 195002
[127] Jost G., Tran T.M., Cooper W.A., Villard L. and Appert K. 2001 *Phys. Plasmas* **8** 3321
[128] Kornilov V., Kleiber R., Hatzky R., Villard L. and Jost G. 2004 *Phys. Plasmas* **11** 3196
[129] Angelino P. *et al* 2006 *Phys. Plasmas* **13** 052304
[130] Garbet X. *et al* 2007 *Nucl. Fusion* **47** 1206
[131] Candy J., Waltz R.E., Parker S.E and Chen Y. 2006 *Phys. Plasmas* **13** 074501
[132] Jolliet S. *et al* 2009 *Phys. Plasmas* **16** 072309
[133] Krommes J.A. 1999 *Phys. Plasmas* **6** 1477
[134] McMillan B.F. *et al* 2008 *Phys. Plasmas* **15** 052308
[135] Chen Y. and Parker S.E. 2007 *Phys. Plasmas* **14** 082301
[136] Candy J. and Waltz R.E. 2006 *Phys. Plasmas* **13** 032310
[137] Terry P.W. *et al* 2008 *Phys. Plasmas* **15** 062503
[138] Greenfield C.M., DeBoo J.C, Osborne T.H., Perkins F.W., Rosenbluth M.N. and Boucher D. 1997 *Nucl. Fusion* **37** 1215
[139] Rosenbluth M.N. and Hinton F.L. 1998 *Phys. Rev. Lett.* **80** 724
[140] Scott B. 2003 *Phys. Lett.* A **320** 53
[141] Beer M.A. and Hammett G.W. 1999 *Proc. Joint Varenna–Lausanne Int. Workshop on Theory of Fusion Plasmas (Varenna, Italy, 1998)* ed J.W. Connor *et al* (Bologna, Italy: Società Italiana de Fisica) p 19
[142] Scott B.D. 2005 *Phys. Plasmas* **12** 102307
[143] Lapillonne X. *et al* 2009 *Phys. Plasmas* **16** 032308
[144] Lin Z., Ethier S., Hahm T.S. and Tang W.M. 2002 *Phys. Rev. Lett.* **88** 195004

[145] Falchetto G.L. *et al* 2008 *Plasma Phys. Control. Fusion* **50** 124015
[146] Peeters A.G. *et al* 2007 *Phys. Rev. Lett.* **98** 265003
[147] Rewoldt G., Tang W.M. and Hastie R.J. 1987 *Phys. Fluids* **30** 807
[148] Rewoldt G., Lin Z. and Idomura Y. 2007 *Comput. Phys. Commun.* **177** 775
[149] Lin Z. *et al* 2005 *Phys. Plasmas* **12** 056125
[150] Nevins W.M. *et al* 2006 *Phys. Plasmas* **13** 122306
[151] Dimits A.M. *et al* 2007 *Nucl. Fusion* **47** 817
[152] Nevins W.M. *et al* 2007 *Phys. Plasmas* **14** 084501
[153] Sydora R.D., Hahm T.S., Lee W.W. and Dawson J.M. 1990 *Phys. Rev. Lett.* **64** 2015
[154] Parker S.E. *et al* 1993 *Phys. Rev. Lett.* **71** 2042
[155] Hammett G.W. *et al* 1993 *Plasma Phys. Control. Fusion* **35** 973
[156] Waltz R.E. *et al* 1994 *Phys. Plasmas* **1** 2229
[157] Parker S.E. *et al* 1994 *Phys. Plasmas* **1** 1461
[158] Dimits A.M. *et al* 1995 *Proc. 15th Int. Conf. on Plasma Physics and Controlled Nuclear Fusion Research 1994 (Seville, Spain, 1994)* vol 3 (Vienna: IAEA) p 457
[159] Ernst D.R. *et al* 2004 *Phys. Plasmas* **11** 2637
[160] Dannert T. and Jenko F. 2005 *Phys. Plasmas* **12** 072309
[161] Peeters A.G. 2005 *Phys. Plasmas* **12** 022505
[162] Mertz T. and Jenko F. 2008 *Phys. Rev. Lett.* **100** 035005
[163] Lang J. *et al* 2008 *Phys. Plasmas* **15** 055907
[164] Jolliet S. 2009 Gyrokinetic particle-in-cell global simulations of ion-temperature-gradient and collisionless-trapped-electron-mode turbulence in tokamaks *PhD Thesis No.4326* Ecole Polytechnique Fédérale de Lausanne
[165] Lin Z. *et al* 2007 *Phys. Rev. Lett.* **99** 265003
[166] Kim J.Y. *et al* 1993 *Phys. Fluids* B **5** 4030
[167] Zonca F. *et al* 1999 *Phys. Plasmas* **6** 1917
[168] Falchetto G.L. *et al* 2003 *Phys. Plasmas* **10** 1424
[169] Pueschel M.J. *et al* 2008 *Phys. Plasmas* **15** 102310
[170] Naitou H. *et al* 1995 *Phys. Plasmas* **2** 4257
[171] Wan W. *et al* 2005 *Phys. Plasmas* **12** 012311
[172] Nishimura Y. *et al* 2007 *Phys. Plasmas* **14** 042503
[173] Zhang W. *et al* 2008 *Phys. Rev. Lett.* **101** 095001
[174] Hauff T., Pueschel M.J., Dannert T. and Jenko F. 2009 *Phys. Rev. Lett.* **102** 075004
[175] Dannert T. *et al* 2008 *Phys. Plasmas* **15** 062508
[176] Howes G.G. *et al* 2006 *Astrophys. J.* **651** 590
[177] Howes G.G. *et al* 2008 *Phys. Rev. Lett.* **100** 065004
[178] Schekochihin A.A. *et al* 2009 *Astrophys. J.* **182** 310
[179] Li J. and Kishimoto Y. 2002 *Phys. Rev. Lett.* **89** 115002
[180] Itoh K. *et al* 2006 *Phys. Plasmas* **13** 055502
[181] Biglari H. *et al* 1990 *Phys. Fluids* B **2** 1
[182] Hahm T.S. and Burrell K.H. 1995 *Phys. Plasmas* **2** 1648
[183] Terry P.W. 2000 *Rev. Mod. Phys.* **72** 109
[184] Hasegawa A., Maclennan C.G. and Kodama Y. 1979 *Phys. Fluids* **22** 2122
[185] Hasegawa A. and Wakatani M. 1987 *Phys. Rev. Lett.* **59** 1581
[186] Dorland W. and Hammett G.W. 1993 *Phys. Fluids* B **5** 812
[187] Cohen B.I. *et al* 1993 *Phys. Fluids* B **5** 2967
[188] Fujisawa A. *et al* 2004 *Phys. Rev. Lett.* **93** 165002
[189] Fujisawa A. 2009 *Nucl. Fusion* **49** 013001
[190] Chen L. *et al* 2000 *Phys. Plasmas* **7** 3129
[191] Diamond P.H. *et al* 1998 *Proc. 17th Int. Conf. on Fusion Energy 1998 (Yokohama, Japan, 1998)* (Vienna: IAEA) CD-ROM file TH3/1 and http://www.iaea.org/programmes/ripc/physics/start.htm
[192] Rogers *et al* 2000 *Phys. Rev. Lett.* **85** 5336
[193] Kim E.-J. and Diamond P.H. 2002 *Phys. Plasmas* **9** 4530
[194] Idomura Y. *et al* 2000 *Phys. Plasmas* **7** 3551
[195] Li J. and Kishimoto Y. 2004 *Phys. Plasmas* **11** 1493
[196] Hallatschek K. 2004 *Phys. Rev. Lett.* **93** 065001
[197] Idomura Y. 2006 *Phys. Plasmas* **13** 080701
[198] Holod I. and Lin Z. 2007 *Phys. Plasmas* **14** 032306
[199] Winsor N. *et al* 1968 *Phys. Fluids* **11** 2448
[200] Lebedev V.B. *et al* 1996 *Phys. Plasmas* **3** 3023
[201] Xu X.Q. 2008 *Phys. Rev. Lett.* **100** 215001
[202] Sugama H. and Watanabe T.-H. 2006 *J. Plasma Phys.* **72** 825
[203] Sugama H. and Watanabe T.-H. 2008 *J. Plasma Phys.* **74** 139
[204] Sugama H. and Watanabe T.-H. 2006 *Phys. Plasmas* **13** 012501
[205] Sugama H. and Watanabe T.-H. 2007 *Phys. Plasmas* **14** 079902
[206] Qiu Z. *et al* 2009 *Plasma Phys. Control. Fusion* **51** 012001
[207] Gao Z. *et al* 2008 *Phys. Plasmas* **15** 074502
[208] Hahm T.S. *et al* 1999 *Phys. Plasmas* **6** 922
[209] Hallatschek K. and Biskamp D. 2001 *Phys. Rev. Lett.* **86** 2001
[210] Miyato N. 2004 *Phys. Plasmas* **11** 5557
[211] Angelino P. *et al* 2006 *Plasma Phys. Control. Fusion* **48** 557
[212] Waltz R.E. and Holland C. 2008 *Phys. Plasmas* **15** 122503
[213] Novakovskii S.V. *et al* 1997 *Phys. Plasmas* **4** 4272
[214] Satake S. *et al* 2007 *Nucl. Fusion* **47** 1258
[215] Hinton F.L. and Rosenbluth M.N. 1999 *Plasma Phys. Control. Fusion* **41** A653
[216] Xiao Y. and Catto P.J. 2006 *Phys. Plasmas* **13** 082307
[217] Belli E.A., Hammett G.W. and Dorland W. 2008 *Phys. Plasmas* **15** 092303
[218] Angelino P. *et al* 2009 *Phys. Rev. Lett.* **102** 195002
[219] Chen Y. *et al* 2003 *Phys. Plasmas* **43** 1121
[220] Kim E.J. *et al* 2003 *Phys. Rev. Lett.* **91** 075003
[221] Xiao Y. and Catto P.J. 2006 *Phys. Plasmas* **13** 102311
[222] Sugama H. *et al* 2007 *Phys. Plasmas* **14** 022502
[223] Lu Wang and Hahm T.S. 2009 *Phys. Plasmas* **16** 062309
[224] Sugama H. and Watanabe T.-H. 2005 *Phys. Rev. Lett.* **94** 115001
[225] Mishchenko A., Helander P. and Könies A. 2008 *Phys. Plasmas* **15** 072309
[226] Watari T., Hamada Y., Fujisawa A., Toi K. and Itoh K. 2005 *Phys. Plasmas* **12** 062304
[227] Ferrando-Margalet S. *et al* 2007 *Phys. Plasmas* **14** 122505
[228] Mynick H.E. and Boozer A.H. 2007 *Phys. Plasmas* **14** 072507
[229] Sugama H. *et al* 2008 *Plasma Fusion Res.* **3** 041
[230] Sugama H. and Watanabe T.-H. 2009 *Phys. Plasmas* **16** 056101
[231] Bak P. *et al* 1987 *Phys. Rev. Lett.* **59** 381
[232] Hwa T. and Karder M. 1992 *Phys. Rev.* A **45** 7002
[233] Diamond P.H. and Hahm T.S. 1995 *Phys. Plasmas* **2** 3640
[234] Sarazin Y. *et al* 2000 *Phys. Plasmas* **7** 1085
[235] Diamond P.H. *et al* 2001 *Nucl. Fusion* **41** 1067
[236] Garbet X. *et al* 2007 *Phys. Plasmas* **14** 122305
[237] Carreras B.A. *et al* 1996 *Phys. Plasmas* **3** 2903
[238] Garbet X. and Waltz R.E. 1998 *Phys. Plasmas* **5** 2836
[239] Sarazin Y. and Ghendrih Ph. 1998 *Phys. Plasmas* **5** 4214
[240] Candy J. and Waltz R.E. 2003 *Phys. Rev. Lett.* **91** 045001
[241] Lin Z. and Hahm T.S. 2004 *Phys. Plasmas* **11** 1099
[242] Hahm T.S. *et al* 2004 *Plasma Phys. Control. Fusion* **46** A323
[243] Waltz R.E. and Candy J. 2005 *Phys. Plasmas* **12** 072303
[244] Sugama H. *et al* 1993 *Proc. 14th Int. Conf. on Plasma Physics and Controlled Nuclear Fusion Research 1992 (Wuerzburg, Germany, 1992)* vol 2 (Vienna: IAEA) p 353
[245] Garbet X. *et al* 1994 *Nucl. Fusion* **34** 963
[246] Chen L. *et al* 2004 *Phys. Rev. Lett.* **92** 075004
[247] Gürcan Ö.D. *et al* 2006 *Phys. Rev. Lett.* **97** 024502
[248] Sánchez R., Newman D.E., Leboeuf J.-N., Decyk V.K. and Carreras B.A. 2008 *Phys. Rev. Lett.* **101** 205002
[249] Sarazin Y. *et al* 2005 *Plasma Phys. Control. Fusion* **47** 1817
[250] Schekochihin A.A. *et al* 2008 *Plasma Phys. Control. Fusion* **50** 124024
[251] Tatsuno T. *et al* 2009 *Phys. Rev. Lett.* **103** 015003
[252] Hammett G.W. and Perkins F.W. 1990 *Phys. Rev. Lett.* **64** 3019
[253] Waltz R.E. *et al* 1992 *Phys. Fluids* B **4** 3138
[254] Beer M. and Hammett G.W. 1996 *Phys. Plasmas* **3** 4046
[255] Sugama H. *et al* 2001 *Phys. Plasmas* **8** 2617
[256] Sugama H. *et al* 2003 *Phys. Plasmas* **10** 726
[257] ITER Physics Basis Expert Group on Confinement and Transport *et al* 1999 *Nucl. Fusion* **39** 2175

[258] Garbet X. and Waltz R.E. 1996 *Phys. Plasmas* **3** 1898
[259] Waltz R.E. *et al* 2002 *Phys. Plasmas* **9** 1938
[260] Parker S.E. 2004 *Phys. Plasmas* **11** 2594
[261] Candy J. 2005 *Phys. Plasmas* **12** 072307
[262] Cordey J.G. *et al* 1999 *Nucl. Fusion* **39** 301
[263] Scott S.D. *et al* 1997 *Proc. 16th Int. Conf. on Fusion Energy 1996 (Montreal, Canada, 1996)* vol 1 (Vienna: IAEA) p 573
[264] Ernst D.R. *et al* 1998 *Phys. Rev. Lett.* **81** 2454
[265] Waltz R.E. *et al* 1997 *Phys. Plasmas* **4** 2482
[266] Hirose A., Livingstone S. and Singh A.K. 2005 *Nucl. Fusion* **45** 1628
[267] Dominguez R.R. and Rosenbluth M.N. 1989 *Nucl. Fusion* **29** 844
[268] Staebler G.M. *et al* 1999 *Phys. Rev. Lett.* **82** 1692
[269] Romanelli F. and Briguglio S. 1990 *Phys. Fluids* B **2** 754
[270] Bourdelle C., Garbet X., Hoang G.T., Ongena J. and Budny R.V. 2002 *Nucl. Fusion* **42** 892
[271] Idomura Y., Tokuda S. and Kishimoto Y. 2005 *Nucl. Fusion* **45** 1571
[272] Candy J., Waltz R.E., Fahey M.R. and Holland C. 2007 *Plasma Phys. Control. Fusion* **49** 1209
[273] Görler T. and Jenko F. 2008 *Phys. Rev. Lett.* **100** 185002
[274] Coppi B. and Spight C. 1978 *Phys. Rev. Lett.* **41** 551
[275] Tang W.M., Rewoldt G. and Chen L. 1986 *Phys. Fluids* **29** 3715
[276] Terry P.W. 1989 *Phys. Fluids* B **1** 1932
[277] Weiland J. 1999 *Collective Modes in Inhomogeneous Plasmas and Advanced Fluid Theory (IOP Series in Plasma Physics)* (London: Taylor and Francis)
[278] Angioni C. *et al* 2003 *Phys. Plasmas* **10** 3225
[279] Garbet X. *et al* 2003 *Phys. Rev. Lett.* **91** 035001
[280] Yankov V.V. 1994 *JETP Lett.* **60** 171
[281] Isichenko M.B., Gruzinov A.V. and Diamond P.H. 1995 *Phys. Rev. Lett.* **74** 4436
[282] Hallatschek K. and Dorland W. 2005 *Phys. Rev. Lett.* **95** 055002
[283] Angioni C. *et al* 2003 *Phys. Rev. Lett.* **90** 205003
[284] Angioni C. and Peeters A.G. 2006 *Phys. Rev. Lett.* **96** 095003
[285] Dubuit N., Garbet X., Parisot T., Guirlet R. and Bourdelle C. 2005 *Phys. Plasmas* **12** 082511
[286] Estrada-Mila C., Candy J. and Waltz R.E. 2005 *Phys. Plasmas* **12** 022305
[287] Angioni C. *et al* 2007 *Phys. Plasmas* **14** 055905
[288] Vlad M., Spineanu F., Itoh S.-I., Yagi M. and Itoh K. 2005 *Plasma Phys. Control. Fusion* **47** 1015
[289] Estrada-Mila C., Candy J. and Waltz R.E. 2006 *Phys. Plasmas* **13** 112303
[290] Angioni C. and Peeters A.G. 2008 *Phys. Plasmas* **15** 052307
[291] Hauff T. and Jenko F. 2008 *Phys. Plasmas* **15** 112307
[292] Rice J.E. *et al* 2007 *Nucl. Fusion* **47** 1618
[293] Dominguez R.R. and Staebler G.M. 1993 *Phys. Fluids* B **5** 3876
[294] Diamond P.H. *et al* 1995 *Proc. 15th Int. Conf. on Plasma Physics and Controlled Nuclear Fusion Research 1994 (Seville, Spain, 1994)* vol 3 (Vienna: IAEA) p 323
[295] Garbet X. *et al* 2002 *Phys. Plasmas* **9** 3893
[296] Peeters A.G. and Angioni C. 2005 *Phys. Plasmas* **12** 072515
[297] Hahm T.S., Diamond P.H., Gürcan Ö.D. and Rewoldt G. 2007 *Phys. Plasmas* **14** 072302
[298] Diamond P.H. *et al* 2008 *Phys. Plasmas* **15** 012303
[299] Peeters A.G. *et al* 2009 *Phys. Plasmas* **16** 042310
[300] Waltz R.E., Staebler G.M., Candy J. and Hinton F.L. 2007 *Phys. Plasmas* **14** 122507
[301] Camenen Y. *et al* 2009 *Phys. Rev. Lett.* **102** 125001
[302] Hahm T.S., Diamond P.H., Gürcan Ö.D. and Rewoldt G. 2008 *Phys. Plasmas* **15** 055902
[303] Gürcan Ö.D., Diamond P.H. and Hahm T.S. 2008 *Phys. Rev. Lett.* **100** 135001
[304] Peeters A.G. *et al* 2009 *Phys. Plasmas* **16** 062311
[305] Wang W.X. *et al* 2009 *Phys. Rev. Lett.* **102** 035002
[306] Holod I. and Lin Z. 2008 *Phys. Plasmas* **15** 092302
[307] Burrell K.H. 1994 *Plasma Phys. Control. Fusion* **36** A291
[308] ASDEX Team 1989 *Nucl. Fusion* **29** 1959
[309] Gohil P. 2006 *C. R. Physique* **7** 606
[310] Stroth U. and Ramisch M. 2006 *C. R. Physique* **7** 686
[311] Wolf R.C. 2003 *Plasma Phys. Control. Fusion* **45** R1
[312] Connor J.W. *et al* 2004 *Nucl. Fusion* **44** R1
[313] Tala T. and Garbet X. 2006 *C. R. Physique* **7** 622
[314] Burrell K.H. 1999 *Phys. Plasmas* **6** 4418
[315] Kinsey J.E., Waltz R.E. and Candy J. 2005 *Phys. Plasmas* **12** 062302
[316] Villard L., Bottino A., Sauter O. and Vaclavik J. 2002 *Phys. Plasmas* **9** 2684
[317] Hinton F.L. and Staebler G.M. 1993 *Phys. Fluids* B **5** 1291
[318] Itoh S.-I., Itoh K., Fukuyama A. and Yagi M. 1994 *Phys. Rev. Lett.* **72** 1200
[319] Lebedev V.B. and Diamond P.H. 1997 *Phys. Plasmas* **4** 1087
[320] Itoh S.-I., Itoh K. and Toda S. 2002 *Phys. Rev. Lett.* **89** 215001
[321] Dif-Pradalier G. *et al* 2008 *Phys. Plasmas* **15** 042315
[322] Ku S. *et al* 2006 *J. Phys.: Conf. Ser.* **46** 87
[323] Scott B.D. *et al* 2008 *Proc. 35th EPS Conf. on Plasma Physics (Hersonissos, Greece)* vol 32D(ECA) P-5.030
[324] Drake J.F. *et al* 1996 *Phys. Rev. Lett.* **77** 494
[325] Beer M.A. *et al* 1997 *Phys. Plasmas* **4** 1792
[326] Bourdelle C. *et al* 2003 *Phys. Plasmas* **10** 2881
[327] Tala T. *et al* 2006 *Nucl. Fusion* **46** 548
[328] Connor J.W., Hastie R.J. and Taylor J.B. 1978 *Phys. Rev. Lett.* **40** 396
[329] Coppi B., Ferreira A., Mark J.W.K. and Ramos J.J. 1979 *Nucl. Fusion* **19** 715
[330] Baranov Y. *et al* 2004 *Plasma Phys. Control. Fusion* **46** 1181
[331] Joffrin E. *et al* 2002 *Plasma Phys. Control. Fusion* **44** 1739
[332] Günter S. *et al* 2001 *Nucl. Fusion* **41** 1283
[333] McDevitt C.J. and Diamond P.H. 2007 *Phys. Plasmas* **14** 112306
[334] Thyagaraja A. *et al* 2004 *Eur. J. Mech. B/Fluids* **23** 475
[335] Waltz R.E., Austin M.E., Burrell K.H. and Candy J. 2006 *Phys. Plasmas* **13** 052301
[336] Miyato N., Kishimoto Y. and Li J.Q. 2007 *Nucl. Fusion* **47** 929
[337] Romanelli F. and Zonca F. 1993 *Phys. Fluids* B **5** 4081
[338] Kishimoto Y. *et al* 1997 *Proc. 16th Int. Conf. on Fusion Energy 1996 (Montreal, Canada, 1996)* vol 2 (Vienna: IAEA) p 581
[339] Kishimoto Y. *et al* 2000 *Nucl. Fusion* **40** 667
[340] Garbet X. *et al* 2001 *Phys. Plasmas* **8** 2793
[341] Garbet X. *et al* 2003 *Nucl. Fusion* **43** 975
[342] Candy J., Waltz R.E. and Rosenbluth M.N. 2004 *Phys. Plasmas* **9** 1879
[343] Chowdhury J. *et al* 2008 *Phys. Plasmas* **15** 072117
[344] Angelino P. *et al* 2008 *Phys. Plasmas* **15** 062306
[345] Hahm T.S., Burrell K.H., Lin Z., Nazikian R. and Synakowski E.J. 2000 *Plasma Phys. Control. Fusion* **42** A205
[346] McKee G.R. *et al* 2003 *Phys. Plasmas* **10** 1712
[347] Conway G.D., Scott B.D. and Schirmer J. 2005 *Plasma Phys. Control. Fusion* **47** 1165
[348] Shats M.G., Xia H. and Yokoyama M. 2006 *Plasma Phys. Control. Fusion* **48** S17
[349] Gupta D.K., Fonck R.J., McKee G.R., Schlossberg D.J. and Shafer M.W. 2006 *Phys. Rev. Lett.* **97** 125002
[350] Itoh S.-I. 2006 Special cluster issue on experimental studies of zonal flow and turbulence *Plasma Phys. Control. Fusion* **48** S1–205
[351] Diamond P.H. *et al* 2000 *Phys. Rev. Lett.* **97** 125002
[352] Holland C. *et al* 2007 *Phys. Plasmas* **14** 056112
[353] Ross D.W. and Dorland W. 2002 *Phys. Plasmas* **9** 5031
[354] Holland C. *et al* 2008 *J. Phys.: Conf. Ser.* **125** 012043
[355] Lin L. *et al* 2009 *Phys. Plasmas* **16** 012502
[356] Casati A. *et al* 2009 *Phys. Rev. Lett.* **102** 165005
[357] White A.E. *et al* 2008 *Phys. Plasmas* **15** 055908

[358] Görler T. and Jenko F. 2008 *Phys. Plasmas* **15** 102508
[359] Hennequin P. *et al* 2004 *Plasma Phys. Control. Fusion* **46** B121
[360] Bourdelle C. *et al* 2007 *Phys. Plasmas* **14** 112501
[361] Kinsey J.E., Staebler G.M. and Waltz R.E. 2008 *Phys. Plasmas* **15** 055908
[362] Barnes M. 2008 Trinity: a unified treatment of turbulence, transport, and heating in magnetized plasmas *PhD Thesis* University of Maryland, http://arxiv.org/pdf/0901.2868
[363] Candy J., Holland C., Waltz R.E., Fahey M.R. and Belli E. 2009 *Phys. Plasmas* **16** 060704